ELSEVIER

MCN Molecular and Cellular Neuroscience

www.elsevier.com/locate/ymcne
Mol. Cell. Neurosci. 35 (2007) 100–108

The TSC1 gene product hamartin interacts with NADE

Sakiko Yasui,[a,1] Kokoro Tsuzaki,[a,1] Haruaki Ninomiya,[a] Florin Floricel,[b] Yasuo Asano,[a] Hirotoshi Maki,[a] Ayumi Takamura,[c] Eiji Nanba,[c] Katsumi Higaki,[c,*] and Kousaku Ohno[b]

[a]*Department of Neurobiology, School of Life Sciences, Tottori University Faculty of Medicine, Yonago 683-8503, Japan*
[b]*Division of Child Neurology, Tottori University Faculty of Medicine, Yonago 683-8503, Japan*
[c]*Division of Functional Genomics, Research Center for Bioscience and Technology, Tottori University, 86 Nishi-machi, Yonago 683-8503, Japan*

Received 29 September 2006; revised 30 January 2007; accepted 6 February 2007
Available online 12 February 2007

Hamartomatous brain lesions are a hallmark of brain pathology of tuberous sclerosis complex (TSC). To elucidate the mechanism of tumor development in the brain of TSC, we identified NADE (p75NTR-associated cell death executor) as an interactor for TSC1 gene product hamartin using a yeast two-hybrid system. In a pull-down assay, endogenous NADE was purified with the immobilized coiled-coil domain (CCD) of hamartin from the PC12h cell lysate. Immunofluorescence and immunoprecipitation confirmed the interaction of hamartin and NADE in cultured neurons and mouse brain lysate. Hamartin constitutively associated with NADE to prevent its proteasomal degradation. Suppression of hamartin with TSC1 small interfering RNA (siRNA) caused reduction of NADE and failed to lead to NGF-induced apoptosis in PC12h cells. These results indicate that hamartin binds to NADE to regulate neuronal cell function and loss of this association is likely to contribute to the brain pathology in TSC.

Keywords: Tuberous sclerosis; Hamartin; Tuberin; NADE; p75NTR; Cell death

Introduction

Tuberous sclerosis complex (TSC) is an autosomal dominant disease occurring in about 1 in 6000 live births with more than half of cases being due to sporadic mutations (Wiederholt et al., 1985; Gomez et al., 1999; Ohno et al., 1999). Individuals affected with TSC develop characteristic abnormalities of the skin (hypomelanotic macules, facial angiofibromas, shagreen patches, fibrous facial plaques), brain (cortical tubers, subependymal nodules, subependymal giant cell astrocytoma), kidney (angiomyolipomas, cysts) and heart (rhabdomyomas) (Gomez et al., 1999). It is hamartomas of the brain that lead to the most severe manifestations of TSC, such as seizure, epilepsy, mental retardation and autism, which cause morbidity and mortality (Mizuguchi and Takashima, 2001; McClintock, 2002; Wiznitzer, 2004; Ess, 2006).

Two causative genes have been identified as tumor suppressor genes, TSC1 on chromosome 9q34 and TSC2 on chromosome 16p13.3, which encode the proteins hamartin and tuberin, respectively (Consortium, 1993; van Slegtenhorst et al., 1997). Allelic loss or loss of heterozygosity (LOH) involving either of the TSC gene loci is demonstrated to result in cerebral, renal and cardiac hamartomas (Sepp et al., 1996; Mizuguchi et al., 2000; Yu et al., 2001; Parry et al., 2001, Sampson, 2003). Hamartin is a ubiquitously expressed 130 kDa protein, which contains a putative transmembrane domain at amino acids 127–144 and a coiled coil domain (CCD) spanning amino acids 719–998 (Consortium, 1993). The amino acid residues 145–510 of hamartin contain the function for activation of Rho GTPase, and amino acid residues 881–1084 interact with the N-terminal of the ezrin–radixin–moezin (ERM) family of actin-binding proteins (Lamb et al., 2000; Goncharova et al., 2004). Hamartin has also been shown to interact with neurofilament-L (Haddad et al., 2002). Tuberin is a 198 kDa ubiquitously expressed protein, which contains a small region of similarity with Rap1 and Rheb GTPase-activating protein (GAP) at amino acids 1593–1631 (Wienecke et al., 1995; Zhang et al., 2003; Saucedo et al., 2003; Li et al., 2004). Tuberin associates with hamartin to inhibit the target of rapamycin (TOR)-mediated signaling to S6 kinase (Inoki et al., 2002; Potter et al., 2002; Gao et al., 2002; Ma et al., 2006). Akt phosphorylates tuberin and inhibits tuberin–hamartin function (Manning et al., 2002; Cai et al., 2006). However, the precise mechanism and relevance of these findings to the pathology of TSC remain unclear. It is likely that hamartin and tuberin have different functions depending on the cell or tissue, therefore identification of additional binding partners for them is essential.

The low affinity neurotrophin receptor (p75NTR) has been shown to mediate the apoptosis signaling under certain condition in neuronal cells (Barker, 2004). p75NTR is a member of the tumor necrosis factor receptor (TNFR) superfamily and contains the death domain motif in its cytoplasmic tail. The cytoplasmic tail is con-

Abbreviations: TSC, tuberous sclerosis complex; CCD, coiled-coil domains; p75NTR, p75 neurotrophin receptor; NADE, p75NTR-associated cell death executor; NGF, nerve growth factor.

* Corresponding author. Fax: +81 859 38 6470.
E-mail address: kh4060@grape.med.tottori-u.ac.jp (K. Higaki).

[1] S. Yasui and K. Tsuzaki contributed equally to this work.

Available online on ScienceDirect (www.sciencedirect.com).

1044-7431/$ - see front matter © 2007 Elsevier Inc. All rights reserved.
doi:10.1016/j.mcn.2007.02.007

sidered to interact with various mediators, such as tumor necrosis factor receptor-associated proteins (TRAFs), zinc finger proteins (SC-1 and NRIF) and RhoA (Chittka and Chao, 1999; Yamashita and Tohyama, 2003; Kenchappa et al., 2006). p75NTR-associated cell death executor (NADE) was identified as a necessary death effector that interacts with the intracellular death domain of p75NTR following the binding of NGF to p75NTR (Mukai et al., 2000). NADE protein is consists of 124 amino acids and has a leucine-rich nuclear export signal (NES) and two boxes for ubiquitination sequences (Kimura et al., 2001). Human NADE is identical to HGR74/Bex3 (Brown and Kay, 1999). NADE contributes to ischemic neurodegeneration in rat hippocampal CA1 neuron and p75NTR-induced cortical neuronal death (Park et al., 2000; Yi et al., 2003). NADE interacts with 14-3-3 proteins to regulate p75NTR-NADE-mediated apoptosis (Kimura et al., 2001). NADE also interacts with second mitochondrial-derived activator of caspase (Smac) to proceed apoptosis (Yoon et al., 2004).

In this study, we identified NADE as a novel interactor protein with hamartin. NADE has been shown to mediate NGF-induced apoptosis in neuronal cells through the interaction with p75NTR (Mukai et al., 2000; Mukai et al., 2002). Hamartin binds to NADE with its CCD domain. Down-regulation of hamartin with TSC1 siRNA led to failure of NGF-induced apoptosis in PC12h cells. Taken together, these results suggest that the association of hamartin with NADE is involved in neuronal cell death, which could explain why hamartoma cells are not eliminated in TSC.

Results

The coiled-coil domain of hamartin interacts with NADE

To identify an interactor for hamartin, the entire span of CCD (amino acid residues 674–1084) was used as a pray (Fig. 1A) and human fetal brain and placenta cDNA libraries were screened as baits by yeast two-hybrid method. Thirteen positive clones from human fetal brain cDNA and 147 positive clones from human placenta cDNA were obtained. Baits sequences from these clones were analyzed with BLAST to seek for homology with known genes. Sequences identical to those encoding for NADE were found to yield positive results and NADE was therefore considered a candidate protein (Supplemental Table S1 and S2). Furthermore, the full length of hamartin CCD was found to be necessary for this interaction since only CCD1 or CCD2 failed to yield positive results (Fig. 1B). The interaction between NADE and TSC1-CCD was confirmed by β-gal assay and a selection assay on auxotrophy for adenine and histidine (Fig. 1B).

Affinity purification of NADE from PC12 cell extract by CCD-GST fused protein

The in vivo screening technique of yeast two-hybrid is known to have a high rate of false positive results. We sought therefore to prove the possible interaction between TSC1 gene product and NADE using an in vitro affinity purification method, namely the GST-fused pull-down assay. Consequently, we expressed the TSC1-CCD as a GST-fused protein (TSC1-CCD-GST) in bacteria. The fusion product was immobilized by glutathione beads and further incubated with PC12h cell lysate. The protein pulled down by TSC1-CCD was subjected to coomasie blue staining and anti-NADE western blotting (Fig. 1C). NADE was pulled-down by TSC1-CCD-GST but not GST.

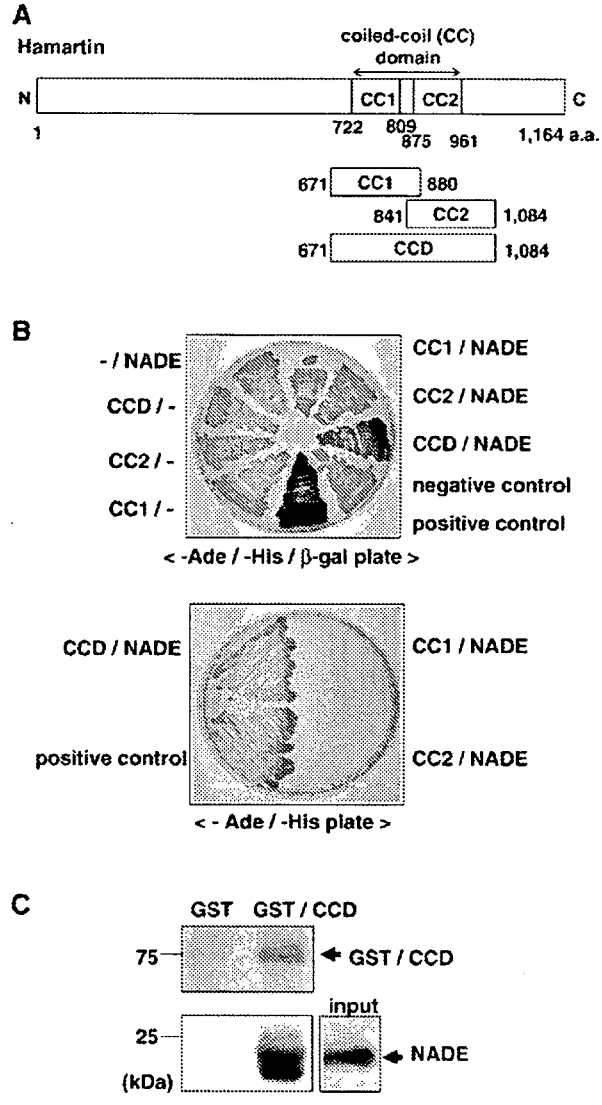

Fig. 1. NADE as a binding partner of hamartin. (A) Construction of hamartin and baits for yeast two-hybrid screening. Upper draw: A primary structure of hamartin with the relative position of the two sub regions of the coiled-coil domain. Lower draw: the amino acid residues span for the regions used as baits; CCD: full length coiled coil domain, CC1: coiled coil domain 1 and CC2: coiled-coil domain 2. (B) NADE interacts with hamartin CCD in yeast. Upper plate: β-gal assay. Lac Z promoter was disrupted by transformation with CC1, CC2, CCD, NADE, CCD1/NADE and CCD2/NADE cDNAs. This loss of suppression recovered after transformation with full length CCD/NADE cDNA. Lower plate: selection on auxotroph for adenine/histidine. Yeast strains AH109 transformed with pGBKT7 vector and Y187 containing pACT2 vector were mated. (C) In vitro interaction of hamartin with NADE. Upper: Proteins bound to GST or CCD/GST were resolved on 12% SDS-PAGE and stained with coomassie blue G-250. Lower: Binding of NADE to CCD/GST fusion protein. Cell extracts from PC12h cells were incubated with GST or CCD/GST beads. Proteins bound to the beads were analyzed by 12% SDS-PAGE and anti-NADE. Molecular weight of CCD/GST is 74 kDa. NADE is 24 kDa. Input: 1% IGEPAL extract from PC12h cells.

Interaction between hamartin and NADE in mammalian cells

We next examined whether forced expression of NADE and TSC1 constructs in a mammalian cell system confirmed this interaction. COS7 cells were co-transfected with pGFP-TSC1 and myc-tagged mouse NADE cDNA (myc-NADE) constructs. Transfection was allowed to proceed overnight and subsequent immunostaining was performed with anti-myc antibody. Detection was realized with Alexa546-conjugated secondary antibody and cells were observed under confocal microscope. Overexpressed GFP-tagged hamartin predominantly localized to cytoplasm, which co-localized with myc-NADE distribution (Fig. 2A). Expression of GFP-hamartin and myc-NADE proteins was confirmed by western blottings (Fig. 2B).

NADE has been shown to associate with p75NTR in PC12 cells (Mukai et al., 2000). Because PC12 cells express detectable levels of p75NTR, NADE, hamartin and tuberin (Catania et al., 2001) and conserve NGF-dependent signaling pathway, we utilized this cell line for further analysis. To substantiate hamartin–NADE interaction, we assayed co-immunoprecipitation of p75NTR, NADE, hamartin and tuberin in PC12h cells. Lysates from cells transfected with p75NTR and myc-NADE were subjected to immunoprecipitation using anti-p75NTR and p75NTR, NADE, hamartin and tuberin were found to co-immunoprecipitate (Fig. 3A). These interactions were further confirmed by immunofluorescence analysis. myc-NADE construct was transiently expressed in PC12h cells and immunofluorescence staining revealed that myc-NADE yielded a diffuse distribution in the cytoplasm and co-localized with p75NTR predominantly in the cytoplasmic region of the plasma membrane. Hamartin and tuberin co-localized with myc-NADE predominantly in the cytoplasm of PC12h cells (Fig. 3B).

Furthermore, we sought to provide a direct evidence of the binding between endogenous hamartin, NADE and tuberin. Extracted lysate from whole mouse brain was immunoprecipitated with ani-hamartin, blotted with anti-hamartin, anti-NADE and anti-tuberin. NADE and tuberin were found to be co-immunoprecipitated with hamartin (Fig. 4A). We also observed that hamartin co-localized with NADE and tuberin in the cytoplasm of primary cultured granule neurons obtained from mouse cerebellum (Fig. 4B).

We next performed immunoprecipitation using crude extract from PC12 cells. Under these conditions, NADE was again found to co-precipitate with hamartin when immunoprecipitation was done with anti-hamartin antibody (Fig. 5A). In previous reports NADE was detected in PC12 cells only after treatment with proteasome inhibitor for 3 h (Mukai et al., 2000). However, we were able to detect NADE co-precipitated with hamartin even in the absence of proteasome inhibitor treatment. (Fig. 5A). We attributed this finding to differences in particular protein concentration between crude lysate and immunoprecipitated material. We also found that the amount of NADE co-precipitate with hamartin did not show any differences with or without NGF and proteasome inhibitor (Fig. 5B). This is in contrast with the amount of NADE co-precipitate with p75NTR. Without NGF and MG132, NADE was degraded by proteasomal system and merely detectable. The quantity of NADE co-precipitate with p75NTR increased after NGF stimulation for 24 h as well as after MG132 treatment for 3 h, the effect of double treatment being additive (Fig. 5B).

Involvement of hamartin and NADE in NGF-dependent cell death pathway

NADE has been shown to associate with the death domain of p75NTR and to promote neuronal cell death after NGF stimulation in PC12 cells (Mukai et al., 2000). Our next step was, therefore, to further study the physiological roles of hamartin and NADE complex. To examine the roles of hamartin in NGF-induced apoptosis, we attempted to reduce the expression of hamartin in PC12h cells using small interference RNA (siRNA). The level of hamartin expression was reduced up to 84% at 24 h after siRNA

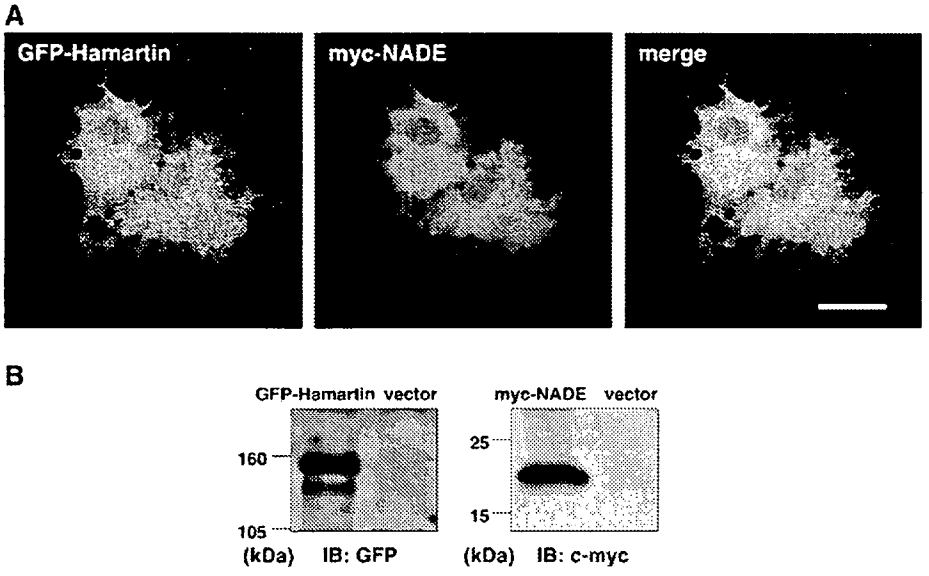

Fig. 2. Co-localization of GFP-hamartin and myc-NADE in COS7 cells. COS7 cells were co-transfected with pGFP-TSC1 and pmyc-NADE expression vectors. (A) Fluorescence images of COS7 cells expressing GFP-tagged hamartin and myc-tagged NADE. Hamartin showed the characteristic pattern in the cytoplasm, which was co-localized with NADE. Scale bar, 30 μm. (B) GFP-hamartin and myc-NADE expressed in COS7 cell were detected by western blotting using anti-GFP and anti-c-*myc* antibodies. Empty vector was used as negative control (vector). Molecular weight of GFP-hamartin and myc-NADE were 160 kDa and 22 kDa, respectively.

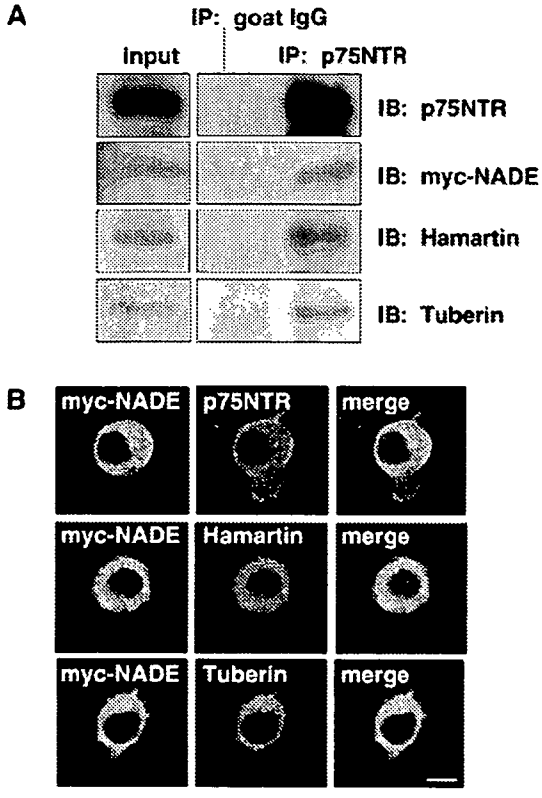

Fig. 3. Co-immunoprecipitation of NADE, hamartin and tuberin with p75NTR in PC12h cells. PC12h cells were co-transfected with p75NTR and myc-NADE expression vectors. (A) Extracted proteins were immunoprecipitated with anti-p75NTR antibody and immunoblotted with anti-p75NTR, anti-NADE, anti-hamartin and anti-tuberin respectively. Normal goat serum was used as a negative control. Input: crude extracts from PC12h cells. (B) Intracellular localization of hamartin, tuberin, NADE and p75NTR. Cells were stained with anti-myc, anti-p75NTR, anti-hamartin and anti-tuberin. NADE co-localized with p75NTR predominantly in cytoplasmic region of the cell membrane. NADE also co-localized with hamartin and tuberin in the cytoplasm. Scale bar, 10 μm.

transfection when compared to the control siRNA transfection (Figs. 6A and B). Immunofluorescence analysis also confirmed the reduction of hamartin expression into the cytoplasma of PC12h cells (Fig. 6C). In addition, levels of NADE were also reduced by TSC1 siRNA transfection (Figs. 6A and B). We examined next the effects of hamartin depletion on NGF-induced cell death. PC12h cells were transfected with NADE and/or TSC1 siRNA for 24 h and were treated with 100 ng/ml NGF for an additional 24 h. Cytotoxic analyses were then performed. Both lactate dehydrogenase (LDH) release assay and annexin-V staining clearly showed that transient transfection of NADE into PC12h cells caused NGF-dependent cell death, whereas this cell death was significantly suppressed in TSC1 siRNA transfected cells (Figs. 6D and E). These results indicate that the reduction of hamartin by siRNA markedly influence NADE/NGF-mediated apoptosis.

Discussion

Hamartomatous brain lesions, such as cortical tubers, subependymal nodules or subependymal giant cell astrocytomas are hallmarks of TSC and results in a variety of neurological manifestations, including mental retardation, seizures and autism (Gomez et al., 1999; McClintock, 2002; Wiznitzer, 2004; Zaroff et al., 2006). Formation of tubers and nodules occurs mainly during brain development, and appears to be complete at the time of birth (Ess, 2006). Analyses with laser capture microdissection or Tsc2 null murine neuroepithelical progenitor have provided evidence of allelic loss in cortical tubers (Mizuguchi et al., 2000; Onda et al., 2002).

In this study, we present four lines of evidence for the interaction between hamartin and NADE. First, NADE was identified as a candidate hamartin interactor from both human fetal brain and placenta cDNA libraries (Fig. 1B). Second, NADE from PC12h cell lysates was affinity-purified by TSC1-CCD (Fig. 1C). Third, hamartin and NADE co-localized in transfected-COS7, PC12h and primary mouse cerebellar granule cells (Figs. 2A, 3A and 4B). Fourth, hamartin was co-precipitated from PC12h cells and mouse brain extracts (Figs. 3A and 4A). These results suggest that NADE is a novel interactor for hamartin and that hamartin possibly participates in p75NTR/NADE-mediated signaling.

The low affinity neurotrophin receptor, p75NTR, is a member of the tumor necrosis factor family and possesses a C-terminal region that is highly homologous to a type-2 death domain that can mediate cell death (Rabizadeh et al., 1993; Frade et al., 1996). p75NTR expression is present throughout the embryonic neural tube development and becomes restricted to post-mitotic cells of the mantle layer, whereas proliferating neuroepitherial cells of the periventricular layer are essentially devoided of o75NTR mRNA and protein (Heuer et al., 1990). Since p75NTR lacks intrinsic enzymatic function, its action is mediated by adaptor proteins such as NADE, NRIF and NRAGE (Kendall et al., 2003). NADE consists of 124 amino acids and lacks any known biochemical motifs except for a nuclear export signal (NES) sequence (Mukai et al., 2000). NADE binds to the intracellular domain of p75NTR in an NGF-dependent manner, and co-expression of NADE and p75NTR induced cell death in HEF293T cells, as well as in PC12 and PC12 nnr5 cells. Expression of p75NTR and NADE was induced in degenerating hippocampal CA1 neurons after forebrain ischemia (Park et al., 2000). NADE has also been shown to interact with dopamine responsive gene-1 (DRG-1) and negatively regulates cell growth of HEK293 and PC12 cells (Yu et al., 2006). In addition, 14-3-3 proteins associate with NADE and play a role in p75NTR/NADE-mediated apoptosis (Kimura et al., 2001). 14-3-3 protein was also shown to be regulated by TSC2 gene product, tuberin (Nellist et al., 2002; Li et al., 2002; Shumway et al., 2003). Tuberin interacts directly with hamartin to form a functional complex (Inoki et al., 2002). Detection of a complex with p75NTR, NADE, hamartin and tuberin (Figs. 2 and 3) suggests that the NADE–hamartin interaction is compatible with hamartin tuberin binding. At this stage of our work, we have no evidence of the direct interaction with tuberin and NADE; however, this interaction may provide additional insight into how the tuerin–hamartin complex functions in p75NTR and PI3K/Akt/mTOR signal transductions.

A possible physiological role for the hamartin–NADE complex was also examined. Expression of NADE has been shown to be detectable within PC12 cells only after treatment with proteasome inhibitors. NADE also interacts transiently with p75NTR after NGF-treatment (Mukai et al., 2000). Here we found here that NADE was constitutively co-precipitated with hamartin without using proteasome inhibitor treatment and its interaction appeared to

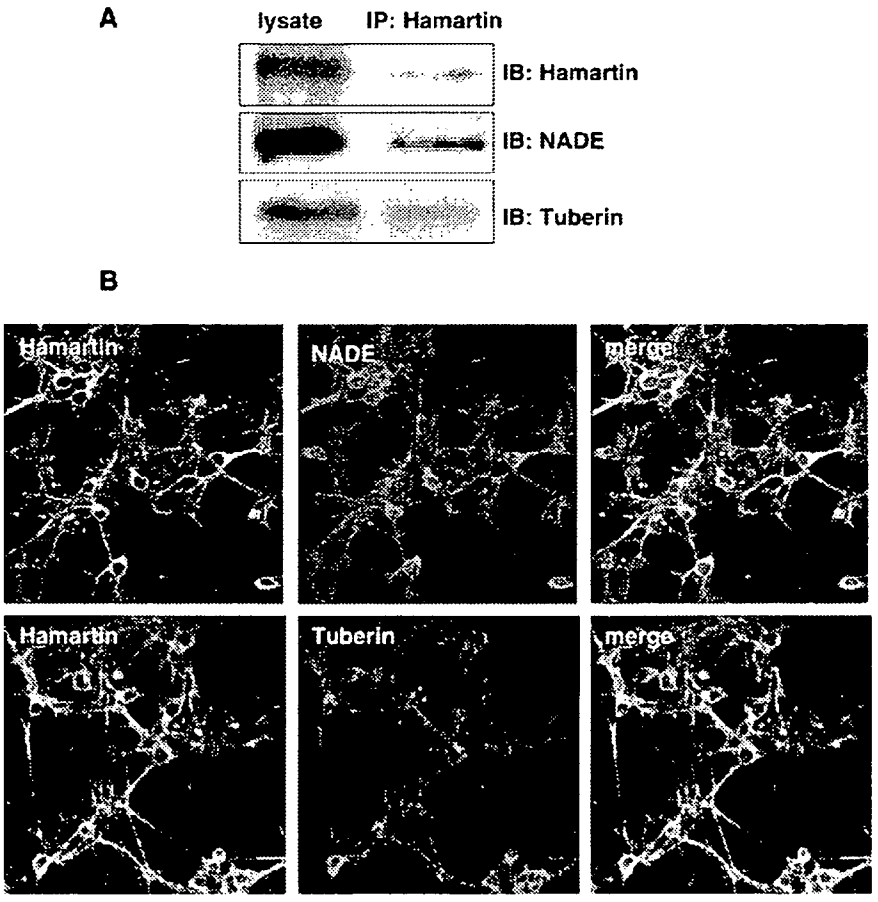

Fig. 4. Interaction between hamartin, NADE and tuberin in the mouse brain. (A) Co-precipitation of anti-hamartin was prepared from the protein extract of normal mouse brain and immunoblotted with anti-hamartin anti-NADE and anti-tuberin. Lysate: crude extracts from mouse brain. (B) Co-localization of hamartin, NADE and tuberin in primary neurons. Primary cerebellar granule cells were prepared as described under Experimental methods. After 7 days culture, cells were stained for hamartin, NADE and tuberin. Scale bar, 20 μm.

be unresponsive to NGF in PC12h cells (Figs. 5A and B). To examine whether suppression of hamartin inhibits NGF-induced cell death, TSC1 siRNA was transfected into PC12h cells. Expression of hamartin was significantly reduced, which caused also the reduction of NADE expression (Figs. 6A–C). As previously reported, PC12h cells were forced into apoptotic death by NGF treatment when NADE was overexpressed (Mukai et al., 2000). Transfection with both NADE and TSC1 siRNA failed to induce NGF-mediated cell death in PC12h cells (Figs. 6D and E). These results suggest that hamartin is possibly involved in p75NTR/NADE-mediated cell death signaling.

In normal brain development, precursors of neuronal cells at the periventricular layer retain the ability of cell division. During corticogenesis, neurons are formed in the ventricular zone and migrate in an orderly fashion to form the hexa-laminar cerebral cortex (Marmur et al., 1998; Nakamura et al., 2003). Analysis of the TSC brain frequently demonstrates focal cortical dysplasia which is suggestive of abnormal neuronal migration or survival (Crino et al., 1996; Kyin et al., 2001). The spectrum of CNS malformations in TSC includes histologic disorganization that spans all layers between the ventricular and marginal zones (Mizuguchi et al., 2001). During normal development, aberrant cells are eliminated by apoptosis, but heterotopic giant cells are found in the subcortical white matter in the cortex of TSC lesions (Gomez et al., 1999). We therefore hypothesized that, if hamartin was involved into p75NTR/NADE-mediated apoptosis, abnormal neural cells in TSC remain in the layers between the ventricular and marginal zones without eliminating by apoptosis. Although the precise mechanisms of these lesions' formation are still to be elucidated, our findings presented herein could explain, at least in part, the reason why abnormal giant cells characteristic of TSC brain lesions are not eliminated.

Experimental methods

Antibodies and reagents

Antibodies against hamartin (rabbit polyclonal IgG), tuberin (C-20, rabbit polyclonal), p75NTR (C-20, goat polyclonal IgG), myc (mouse monoclonal IgG) and caspase-3 (E-8, mouse monoclonal) were from Santa Cruz biotech. Inc. (Santa Cruz, CA), mouse monoclonal anti-hamartin antibody was from BD Biosciences (Franklin Lakes, NJ). Anti-NADE antibody (rabbit polyclonal IgG) was kindly provided by Dr. Taka-Aki Sato (Columbia University, NY). The collagen type IV was from Sigma (St. Louis, MO), the proteasome inhibitor MG132 was from Calbiochem (San Diego, CA) and the murine NGF (nerve growth factor) 2.5S was from Wako (Tokyo, Japan).

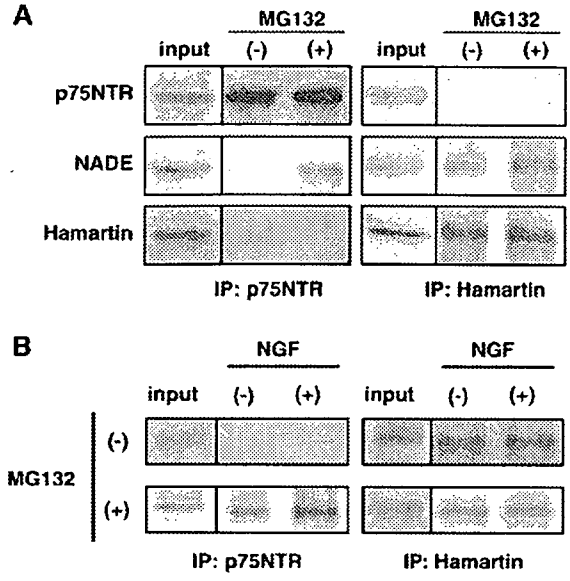

Fig. 5. Association of NADE with hamartin in PC12h cells. (A) Immunoprecipitation with anti-p75NTR and anti-hamartin antibodies from PC12h cells extract. PC12h cells were collected after being treated or not treated with MG132. Immunoprecipitated proteins were blotted with anti-p75NTR, anti-NADE and anti-hamartin, respectively. (B) PC12h cells were cultured with or without NGF for 24 h. Cells were also treated with or without MG132 for 3 h before harvest. Extracted proteins were immunoprecipitated with anti-p75NTR or anti-hamartin and immunoblotted with anti-NADE antibody. Input: crude extracts from PC12h cells.

Mammalian and bacterial expression constructs

To generate mammalian expression of N-terminal green fluorescence protein (GFP)-tagged hamartin protein (pGFP-TSC1), human full length TSC1 cDNA was obtained by RT-PCR from the HEK293 RNA using the following primers (hTSC1-F: 5′-GCGGCCGCATGGCCCAACAAG-CAAATGT-3′, hTSC1-R: 5′-GCGGCCGCTTAGCAGTGTTCATGAT-GAG-3′) and then cloned into pEGFP-C1 vector (Clontech). cDNAs encoding for coiled-coil domain 1 (CC1; 671–880 aa), coiled-coil domain 2 (CC2; 841–1084 aa) and full coiled-coil domain (CCD; 671–1084 aa) were amplified using primers (CC1-F: 5′-CATATGAGCAAGTCTGTCGACTG-GACCCAC-3′, CC1-R: 5′-GGATCCCATCATTTCTACTTCCTTTGT-GGT-3′, CC2-F: 5′-CATATGGTCCAGCAGCAGATGGAGTTCTTG-3′, CC2-R: 5′-GGATCCTGAACTGGGAAGTGAGCCCACAGT-3′), inserted into pGEX-6p-1 (Amersham Bioscience, GE Healthcare Bio-Sciences Corp., Piscataway, NJ) and used for bacterial expression. Mammalian expression construct of c-*myc*/His tagged-mouse NADE cDNA (pcDNA3.1/myc-his(-)A/mouse-NADE) was a gift from Dr. Taka-Aki Sato (Mukai et al., 2000). All constructs were confirmed by sequencing (ABI 3130).

Yeast two-hybrid screening

The Matchmaker two-hybrid system was obtained from Clontech (Invitrogen, Carlsbad, CA) and GAL4 two-hybrid system was carried out following the manufacturer's instruction. Human TSC1-CCD cDNA encoding 414 amino acids was cloned into pGBKT7 in fusion with the yeast Gal4 DNA binding domain and transformed into MATa AH109 strain. Expression of the hybrid protein was verified by western blotting with anti-c-*myc* (data not shown). cDNA libraries used for screening were from human fetal brain and placenta, cloned at the *Xho*I/*Eco*RI site of pACT2 as a fusion with the Gal4 activation domain. These libraries were transformed into MAT1α Y187 strain. Pretransformed bait and library cultures were mated to each other. Mating cultures were plated onto selection medium lacking tryptophan, leucine, histidine and adenine. Surviving colonies larger than 2 mm in diameter were collected and re-streaked on the same medium. Colonies that regrew were further tested for β-galactosidase activity using a liquid β-gal assay according to the manufacturer's protocol. The plasmid DNAs were isolated from positive yeast colonies, and *E. coli* DH5α (TOYOBO, Tokyo, Japan) was utilized to amplify the cDNAs. The inserted cDNAs were prepared for DNA sequencing with the following primers (ACT2-F: 5′-TACCACTACAATGGATG-3′, ACT2-R: 5′-GTGAACTTGCGGGGTTTTTCAGTATCTACG-3′). Obtained sequences were searched for homologous gene with NCBI BLAST. For two-hybrid protein–protein interaction assay, the full length NADE cDNA was cloned in to pACT2 at the *Xho*I/*Eco*RI site and transformed into yeast strain AH109. In addition, hamarin-CC1, hamartin-CC2 and hamartin-CCD fragments were cloned into pGBKT7 and transformed into yeast strain Y187. The pACT2/NADE strain was mated to pGBKT7/CC1, pGBKT7/CC2 or pGBKT7/CCD strains, respectively. For the surviving mating cultures, nutrition selection and liquid β-gal assay were performed as described above.

GST pull-down assay

GST and GST-CCDs were expressed in XL-10 GOLD ultra competent cells (Stratagen). Transformed cells were grown in the presence of 1 mM isopropyl-1-thio-β-D-galactopyrsnoside (IPTG) for 1 h at 37 °C. Bacterial pellet was lysed by sonication in buffer A (50 mM Tris–HCl pH 8.0, 50 mM NaCl, 1 mM EDTA, 5 mM DTT, protease inhibitor cocktail (Roche), 1% Triton X-100) and the lysate was centrifuged at 15,000 rpm for 10 min at 4 °C. The supernatant was recovered and spun down for an additional 30 min. Pellet containing inclusion bodies was then washed with buffer B (1 mM EDTA, 1% Triton X-100) and the inclusions were lysed in 8 M urea buffer (8 M urea, 50 mM Tris–HCl pH 8.0, 5 mM DTT, 1 mM EDTA). After centrifugation at 13,000 rpm for 30 min at 4 °C, the supernatant was dialyzed against buffer A (without proteasome inhibitory cocktail) to remove urea. Glutathione Sepharose 4B beads (Amersham Bioscience) were loaded onto columns (Bio-Rad) and washed once with buffer A. GST and GST-CCD protein samples were then loaded onto columns and the coupling reaction was allowed to proceed for 2 days at 4 °C. Columns were then washed 2 times with buffer A and PC12h cell lysate was then loaded into the columns and incubated overnight at 4 °C. The columns were washed three times with buffer A. Bound proteins were eluted by 10 mM reduced glutathione and subsequently analyzed by western blotting and Coomasie-blue staining.

Cell culture and transfection

Human embryonic kidney cell line, HEK 293, and monkey kidney cell line, COS7 cells, were maintained in Dulbecco's modified Eagle's medium (DMEM; Sigma, St Louis, MO) with 10% fetal bovine serum (FBS; HyClone, Logan, UT). Rat pheochromocytoma cell line, PC12h, was maintained in DMEM supplemented with 5% FBS and 5% heat-inactivated horse serum (Gibco) as previously described (Yamazaki et al., 2004). Transfections of mammalian expression vectors were performed with LipofectAmine Plus (Invitrogen) or FuGene-6 (Roche) transfection reagents following manufacturer's instructions. For immunoprecipitation, PC12h cells cultured on collagen IV coated dishes at 70% confluence, transfected with myc-NADE and allowed to proceed overnight. Then medium was replaced by serum-free DMEM supplemented with 50 (or 100) ng/ml NGF and incubated for an additional 24 h. We obtained rat TSC1 siRNA from Qiagen (^{126}AAACACGTTGGTGAATTATTA^{146}). Transfection of siRNA into PC12h cells was performed using Lipofectamine 2000 (Invitrogen) according to the manufacture's protocol. Scrambled siRNA was used as a control.

Co-precipitation and western blotting

Intact PC12h or transfected cells were lysed in IP buffer (10 mM Tris–HCl pH 7.4, 150 mM NaCl, 1 mM EDTA, 1 mM EGTA, 100 mM NaF,

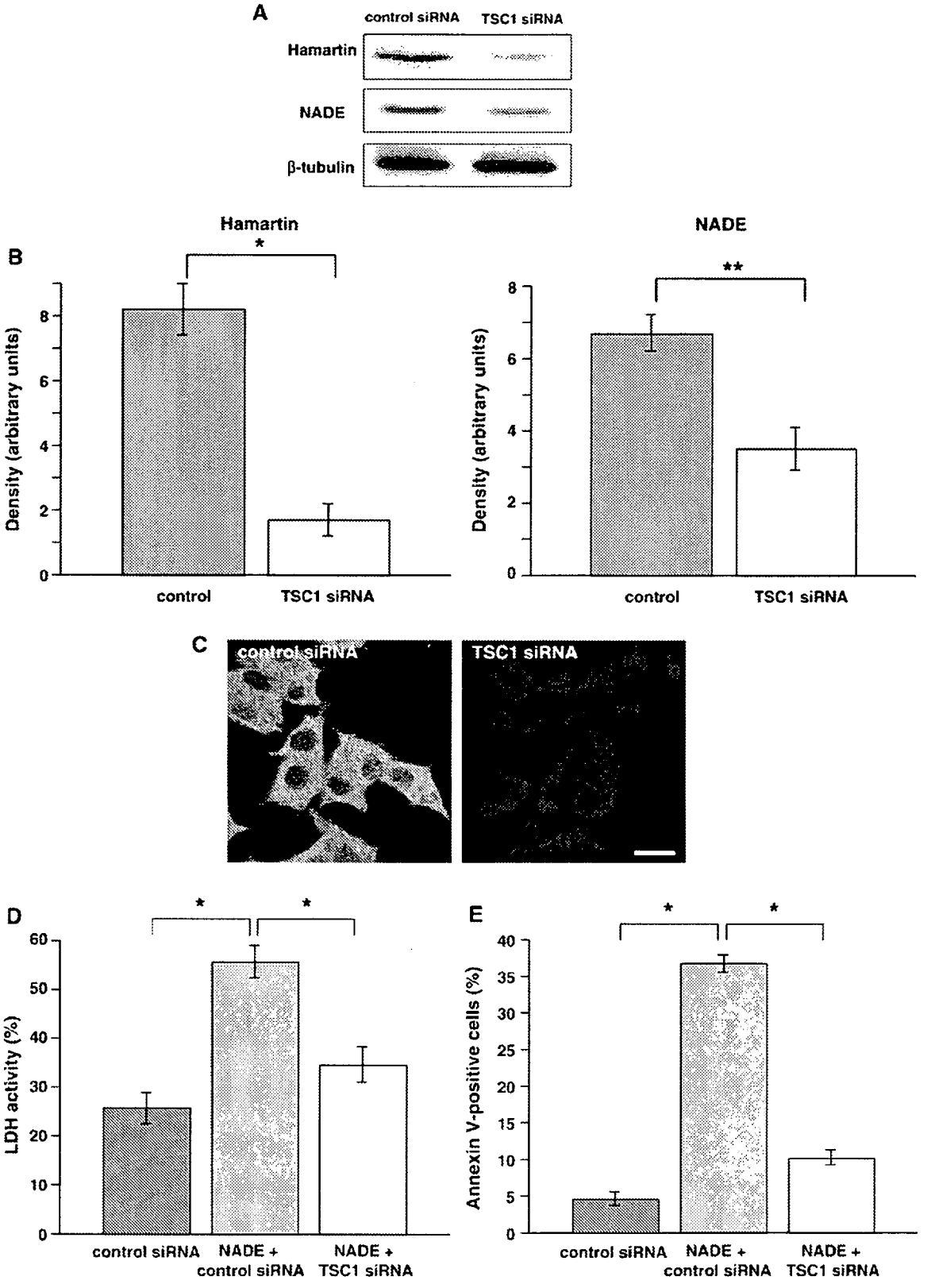
A
control siRNA
TSC1 siRNA
Hamartin
NADE
β-tubulin
B
Hamartin
*
Density (arbitrary units)
control
TSC1 siRNA
NADE
**
Density (arbitrary units)
control
TSC1 siRNA
C
control siRNA
TSC1 siRNA
D
*
*
LDH activity (%)
control siRNA
NADE + control siRNA
NADE + TSC1 siRNA
E
*
*
Annexin V-positive cells (%)
control siRNA
NADE + control siRNA
NADE + TSC1 siRNA

1 mM Na_3VO_4, proteinase inhibitor cocktail and 1% IGEPAL) and immunoprecipitated with anti-p75NTR or anti-hamartin antibody coupled to Protein A Sepharose 4 Fast Flow (Amersham Bioscience). Immunocomplexes were subjected to SDS-PAGE and transferred to PVDF membrane (Millipore, Bedford, MA). Membranes were blocked in Block Ace (Yulijirushi, Japan) for 1 h at room temperature, incubated overnight at 4 °C with primary antibody. Membranes were then incubated with horseradish peroxidase-fused secondary antibody for 1 h at room temperature. Detection was carried out using ECL detection system (Amersham Pharmacia). Normal mouse brain extract was obtained from 3 months old mice (C57BL/6 strain), lysed in IP buffer and immunoprecipitated with anti-hamartin as described above.

Primary cerebellar granule cell culture

Primary cerebellar granule cells were isolated from brains of 8 day-old C57BL/6 mice and dissociated with trypsin-DNase by Pasteur pipette trituation (Canu et al., 2005). Cells were plated at the number of 2×10^5 cells in 35 mm dishes with poly-L-lysine coated glass coverslips and maintained in DMEM/F12 (Sigma) supplemented with 10% FBS, 25 mM KCl, 10 mg/ml gentamicin and 20 mM cytosine arabinoside for 7 days. Cells were fixed in 4% paraformaldehyde in PBS for 30 min and stained with antibodies as described below.

Immunofluorescence

COS7 or PC12h cells were inoculated on 35 mm dishes with cover slips and incubated overnight. The following day they were washed with PBS, fixed with 4% paraformaldehyde in phosphate-buffered saline (PBS) for 30 min, permeabilized with 0.25% Triton X-100 in PBS for 10 min and then incubated with 1% bovine serum albumin (BSA) in PBS for 1 h at room temperature. Primary antibody (dilution with 0.1% BSA/PBS) was applied overnight at 4 °C, bound antibodies were detected with Alexa Fluor-conjugated secondary antibodies (diluted with 1:2000 in 0.1% BSA/PBS; Molecular Probes). Fluorescence images were obtained using confocal microscopy (Leica, TCS SP-2).

Cytotoxicity assay

Cytotoxicity assays were performed in lactate dehydrogenase (LDH) assay and annexin-V staining. Transfected PC12h cells were treated with NGF for 24 h. LDH assay was performed using LDH assay kit (WAKO, Tokyo, Japan) by measuring LDH activity released into the medium. Medium was filtrated through 0.45 μm-pore filters and subjected to the assay. Values were calculated as relative to the values from cells lysed with 1% Tween 20. For annexin-V staining, apoptotic cells were labeled by incubating with annexin-V FITC solution (Sigma, St. Louis, MO) for 10 min at room temperature as following the manufacturer's protocol. The number of annexin-V FITC-positive cells was quantified under fluorescence microscopy (Leica, DMIRE2).

Acknowledgments

We thank Drs. Taka-Aki Sato and Jun Mukai for anti-NADE antibody and NADE cDNA expression construct. This research was partially supported by the Ministry of Health, Labour and Welfare of Japan. F. Floricel was supported by a Japanese Government research scholarship from the Japan Ministry of Education, Culture, Sports, Science and Technology.

Appendix A. Supplementary data

Supplementary data associated with this article can be found, in the online version, at doi:10.1016/j.mcn.2007.02.007.

References

Barker, P.A., 2004. p75NTR is positively promiscuous: novel partners and new insights. Neuron 42, 529–533.

Brown, A.L., Kay, G.F., 1999. Bex1, a gene with increased expression in parthenogenetic embryos, is a member of a novel gene family of the mouse X chromosome. Hum. Mol. Genet. 8, 611–619.

Cai, S.L., Tee, A.R., Short, J.D., Bergeron, J.M., Kim, J., Shen, J., Guo, R., Johnson, C.L., Kiguchi, K., Walker, C.L., 2006. Activity of TSC2 is inhibited by AKT-mediated phosphorylation and membrane partitioning. J. Cell Biol. 173, 279–289.

Canu, N., Tufi, R., Serafino, A.L., Amadoro, G., Ciotti, M.T., Calissano, P., 2005. Role of the autophagic-lysosomal system on low potassium-induced apoptosis in cultured cerebellar granule cells. J. Neurochem. 92, 1228–1242.

Catania, M.G., Johnson, M.W., Liau, L.M., Kremen, T.J., deVellis, J.S., Vinters, H.V., 2001. Hamartin expression and interaction with tuberin in tumor cell lines and primary cultures. J. Neurosci. Res. 63, 276–283.

Chittka, A., Chao, M.V., 1999. Identification of a zinc finger protein whose subcellular distribution is regulated by serum and nerve growth factor. Proc. Natl. Acad. Sci. U. S. A. 96, 10705–10710.

Consortium (The European Chromosome 16 Tuberous Sclerosis Consortium), 1993. Tuberous sclerosis gene on chromosome 16. Cell 75, 1305–1315.

Crino, P.B., Trojanowski, J.Q., Dichter, M.A., Eberwine, J., 1996. Embryonic neuronal markers in tuberous sclerosis: single-cell molecular pathology. Proc. Natl. Acad. Sci. U. S. A. 93, 14152–14157.

Ess, K.C., 2006. The neurobiology of tuberous sclerosis complex. Semin. Pediatr. Neurol. 13, 37–42.

Frade, J.M., Rodriguez-Tebar, A., Barde, Y.A., 1996. Induction of cell death by endogenous nerve growth factor through its p75 receptor. Nature 383, 166–168.

Gao, X., Zhang, Y., Arrazola, P., Hino, O., Kobayashi, T., Yeung, R.S., Ru, B., Pan, D., 2002. Tsc tumor suppressor proteins antagonize amino-acid-TOR signaling. Nat. Cell Biol. 4, 699–704.

Gomez, M.R., Sampson, J.R., Wittemore, V.H., 1999. Tuberous Sclerosis Complex, 3rd ed. Oxford University Press, New York.

Goncharova, E., Goncharov, D., Noonan, D., Krymskaya, V.P., 2004. TSC2 modulates actin cytoskelton and focal adhesion through TSC1-binding domain and the Rac1 GTPase. J. Cell Biol. 167, 1171–1182.

Haddad, L.A., Smith, N., Bowser, M., Niida, Y., Murthy, V., Gonzalez-Agosti, C., Ramesh, V., 2002. The TSC1 tumor suppressor hamartin interacts with neurofilament-L and possibly functions as a novel integrator of the neuronal cytoskelton. J. Biol. Chem. 277, 44180–44186.

Heuer, J.G., von Bartheld, C.S., Kinoshita, Y., Evers, P.C., Bothwell, M., 1990. Alternating phases of FGF receptor and NGF receptor expression in the developing chicken nervous system. Neuron 5, 283–296.

Fig. 6. Suppression of hamartin failed to NGF-induced cell death in PC12h cells. (A) Protein extracts were prepared from siRNA transfected PC12h cells and blotted with anti-hamartin, anti-NADE and anti-β-tubulin (as loading control). (B) Quantification of hamartin (left panel) and NADE (right panel) immunoreactivities. (C) PC12h cells were transfected with control or rat TSC1 siRNA. After 24 h transfection, cells were stained with anti-hamartin. Scale bar, 20 μm. (D) Lactate dehydrogenase (LDH) release assay. PC12h cells were transfected with control or TSC1 siRNA and/or myc-NADE expression vector. Cells were treated with 100 ng/ml NGF for 24 h and examined for the assay. Values were expressed as relative to the values from cells with 1% Tween 20. (E) Annexin-V staining. Annexin-V positive cells were counted under the fluorescence microscopy. Values were expressed the percentage relative to the total number of the cells. Values are mean±SEM, $n=3$, $^*p<0.01$, $^{**}p<0.05$.

Inoki, K., Li, Y., Zhu, T., We, J., Guan, K.L., 2002. TSC2 is phosphorylated and inhibited by Akt and suppresses mTOR signaling. Nat. Cell Biol. 4, 648–657.

Kenchappa, R.S., Zampieri, N., Chao, M.V., Barker, P.A., Teng, H.K., Hempstead, B.L., Carter, B.D., 2006. Ligand-dependent cleavage of the p75 neurotrophin receptor is necessary for NRIF nuclear translocation and apoptosis in sympathetic neurons. Neuron 50, 219–232.

Kendall, S.E., Ryczko, M.C., Mehan, M., Verdi, J.M., 2003. Characterization of NADE, NRIF and SC-1 gene expression during mouse neurogenesis. Dev. Brain Res. 144, 151–158.

Kimura, M.T., Irie, S., Shoji-Hoshino, S., Mukai, J., Nadano, D., Oshimura, M., Sato, T.A., 2001. 14-3-3 is involved in p75 neurotrophin receptor-mediated signal transduction. J. Biol. Chem. 276, 17291–17300.

Kyin, R., Hua, Y., Baybis, M., Scheithauer, B., Kolson, D., Uhlmann, E., Gutmann, D., Crino, P.B., 2001. Differential cellular expression of neurotrophin in cortical tubers of the tuberous sclerosis complex. Am. J. Pathol. 159, 1541–1554.

Lamb, R.F., Roy, C., Diefenbach, T.J., Vinters, H.V., Johnson, M.W., Jay, D.G., Hall, A., 2000. The TSC1 tumor suppressor hamartin regulates cell adhesion through ERM proteins and the GTPase Rho. Nat. Cell Biol. 2, 281–287.

Li, Y., Inoki, K., Yeung, R., Guan, K.L., 2002. Regulation of TSC2 by 14-3-3 binding. J. Biol. Chem. 277, 44593–44596.

Li, Y., Inoki, K., Guan, K.L., 2004. Biochemical and functional characterizations of small GTPase Rheb and TSC2 GAP activity. Mol. Cell Biol. 24, 7965–7975.

Ma, L., Chen, Z., Erdjument-Bromage, H., Tempst, P., Pandolfi, P.P., 2006. Phosphorylation and functional inactivation of TSC2 by Erk implications for tuberous sclerosis and cancer pathogenesis. Cell 121, 179–193.

Manning, B.D., Tee, A.R., Logsdon, M.N., Blenis, J., Cantley, L.C., 2002. Identification of the tuberous sclerosis complex-2 tumor suppressor gene product tuberin as a target of the phosphoinositide-3-kinase/akt pathway. Mol. Cell 10, 151–162.

Marmur, R., Mabie, P.C., Gokhan, S., Song, Q., Kessler, J.A., Mehler, M.F., 1998. Isolation and developmental characterization of cerebral cortical multipotent progenitors. Dev. Biol. 204, 577–591.

McClintock, W.M., 2002. Neurologic manifestations of tuberous sclerosis complex. Curr. Neurol. Neurosci. Rep. 2, 158–163.

Mizuguchi, M., Takashima, S., 2001. Neuropathology of tuberous sclerosis. Brain Dev. 23, 508–515.

Mizuguchi, M., Ikeda, K., Takashima, S., 2000. Simultaneous loss of hamartin and tuberin from the cerebrum, kidney and heart with tuberous sclerosis. Acta Neuropathol. 99, 503–510.

Mukai, J., Hachiya, T., Shoji-Hoshino, S., Kimura, M.T., Nadano, D., Suvanto, P., Hanaoka, T., Li, Y., Irie, S., Greene, L.A., Sato, T.A., 2000. NADE, a p75NTR-associated cell death executor, is involved in signal transduction mediated by the common neurotrophin receptor p75NTR. J. Biol. Chem. 275, 17566–17570.

Mukai, J., Shiji, S., Kimura, M.T., Okubo, S., Sano, H., Suvanto, P., Li, Y., Irie, S., Sato, T.A., 2002. Structure-function analysis of NADE. J. Biol. Chem. 227, 13973–13982.

Nakamura, Y., Yamamoto, M., Oda, E., Yamamoto, A., Kanemura, Y., Hara, M., Suzuki, A., Yamasaki, M., Okano, H., 2003. Expression of tubulin beta II in neural stem/progenitor cells and radial fibers during human fetal brain development. Lab. Invest. 83, 479–489.

Nellist, M., Goedbloed, M.A., de Winter, C., Verhaaf, B., Jankie, A., Reuser, A.J., van den Ouweland, A.M., van der Sluijs, P., Halley, D.J., 2002. Identification and characterization of the interaction between tuberin and 14-3-3zeta. J. Biol. Chem. 277, 39417–39424.

Ohno, K., Yakura, N., Zhang, H., Ninomiya, H., Nanba, E., 1999. Molecular epidemiology of tuberous sclerosis. In: Niimura, M., Otsuka, F., Hino, O. (Eds.), Phacomatosis in Japan-epidemiology, Clinical Picture, and Molecular Biology. Japan Scientific Societies Press, Tokyo, pp. 53–59.

Onda, H., Crino, P.B., Zhang, H., Murphey, R.D., Rastelli, L., Gould-Rothberg, B.E., Kwiatkowski, D.J., 2002. Tsc2 null murine neuroepithelial cells are a model for human tuber giant cells, and show activation of an mTOR pathway. Mol. Cell Neurosci. 21, 561–574.

Park, J.A., Lee, J.Y., Sato, T.A., Koh, J.Y., 2000. Co-induction of p75NTR and p75NTR-associated death executor in neurons after zinc exposure in cortical culture or transient ischemia in the rat. J. Neurosci. 20, 9096–9103.

Parry, L., Maynard, J.H., Patel, A., Clifford, S.C., Morrissey, C., Maher, E.R., Cheadle, J.P., Sampson, J.R., 2001. Analysis of the TSC1 and TSC2 gene in sporadic renal cell carcinoma. Br. J. Cancer 85, 1226–1230.

Potter, C.J., Pedraza, L.G., Xu, T., 2002. Akt regulates growth by directly phosphorylating Tsc2. Nat. Cell. Biol. 4, 658–665.

Rabizadeh, S., Oh, J., Zhong, L.T., Yang, J., Bitler, C.M., Butcher, L.L., Bredesen, D.E., 1993. Induction of apoptosis by the low-affinity NGF receptor. Science 261, 345–348.

Sampson, J.R., 2003. TSC1 and TSC2 genes that are mutated in the human genetic disorder tuberous sclerosis. Biochem. Soc. Trans. 31, 592–596.

Saucedo, L.J., Gao, X., Chiarelli, D.A., Li, L., Pan, D., Edgar, B.A., 2003. Rheb promotes cell growth as a component of the insulin/TOR signaling network. Nat. Cell Biol. 5, 566–571.

Sepp, T., Yates, J.R., Green, A.J., 1996. Loss of heterozygosity in tuberous sclerosis hamartomas. J. Med. Genet. 33, 962–966.

Shumway, S.D., Li, Y., Xiong, Y., 2003. 14-3-3beta binds to and negatively regulates the tuberous sclerosis complex 2 (TSC2) tumor suppressor gene product, tuberin. J. Biol. Chem. 278, 2089–2092.

van Slegtenhorst, M., dde Hoogt, R., Hermans, C., Nellist, M., Janssen, B., Verhoef, S., Lindhout, D., et al., 1997. Identification of the tuberous sclerosis gene TSC1 on chromosome 9q34. Science 277, 805–808.

Wiederholt, W.C., Gomez, M.R., Kurland, L.T., 1985. Incidence and prevalence of tuberous sclerosis in Rochester, Minnesota, 1950 through 1982. Neurology 35, 600–603.

Wienecke, R., Konig, A., DeClue, J.E., 1995. Identification of tuberin, the tuberous sclerosis-2 product. Tuberin possesses specific Rap1GAP activity. J. Biol. Chem. 270, 16409–16414.

Wiznitzer, M., 2004. Autism and tuberous sclerosis. J. Child Neurol. 19, 675–679.

Yamashita, T., Tohyama, M., 2003. The p75 receptor acts as a displacement factor that releases Rho from Rho-GDI. Nat. Neurosci. 6, 461–467.

Yamazaki, M., Chiba, K., Mohri, T., Hatanaka, H., 2004. Cyclic GMP-dependent neurite outgrowth by genipin and nerve growth factor in PC12h cells. Eur. J. Pharmacol. 488, 35–43.

Yi, J.S., Lee, S.K., Sato, T.A., Koh, J.Y., 2003. Co-induction of p75NTR and the associated death executor NADE in degenerating hippocampal neurons after kinate-induced seizures in the rat. Neurosci. Lett. 347, 126–130.

Yoon, K., Jang, H.D., Lee, S.Y., 2004. Direct interaction of Smac with NADE promotes TRAIL-induced apoptosis. Biochem. Biophys. Res. Commun. 319, 649–654.

Yu, J., Astrinidis, A., Henske, E.P., 2001. Chromosome 16 loss of heterozytosity in tuberous sclerosis and sporadic lymphangiomyomatosis. Am. J. Respir. Crit. Care Med. 164, 1537–1540.

Yu, Y., Wang, J., Yuan, H., Qin, F., Wang, J., Zhang, N., Li, Y.Y., Liu, J., Lu, H., 2006. Characterization of human dopamine responsive protein DRG-1 that binds to p75NTR-associated cell death executor NADE. Brain Res. 1100, 13–20.

Zaroff, C.M., Barr, W.B., Carlson, C., LaJoie, J., Madhavan, D., Miles, D.K., Nass, R., Devinsky, O., 2006. Mental retardation and relation to seizure and tuber burden in tuberous sclerosis complex. Seisure 15, 558–562.

Zhang, Y., Gao, X., Saucedo, L.J., Ru, B., Edgar, B.A., Pan, D., 2003. Rheb is a direct target of the tuberous sclerosis tumor suppressor proteins. Nat. Cell Biol. 5, 578–581.

ELSEVIER

Brain & Development 29 (2007) 510–513

BRAIN & DEVELOPMENT
Official Journal of the Japanese Society of Child Neurology

www.elsevier.com/locate/braindev

Original article

Tachykinin 1 (TAC1) gene SNPs and haplotypes with autism: A case-control study

Tetsuya Marui [a,*], Ikuko Funatogawa [b], Shinko Koishi [c], Kenji Yamamoto [d], Hideo Matsumoto [e], Ohiko Hashimoto [f], Eiji Nanba [g], Hisami Nishida [h], Toshiro Sugiyama [c], Kiyoto Kasai [a], Keiichiro Watanabe [i], Yukiko Kano [i], Nobumasa Kato [a], Tsukasa Sasaki [a,j]

[a] *Department of Neuropsychiatry, Graduate School of Medicine, University of Tokyo, Tokyo, Japan*
[b] *Department of Hygiene and Public Health, Teikyo University School of Medicine, Tokyo, Japan*
[c] *Aichi Children's Health and Medical Center, Obu, Japan*
[d] *Department of Psychiatry, Kitasato University School of Medicine, Sagamihara, Japan*
[e] *Department of Psychiatry, Tokai University School of Medicine, Isehara, Japan*
[f] *Department of Occupational Therapy, Faculty of Nursing and Rehabilitation, Aino University, Ibaraki, Japan*
[g] *Gene Research Center, Tottori University, Yonago, Japan*
[h] *Asunaro Hospital for Child and Adolescent Psychiatry, Tsu, Japan*
[i] *Department of Child Psychiatry, School of Medicine, University of Tokyo, Tokyo, Japan*
[j] *Department of Psychiatry, Health Service Center, University of Tokyo, Tokyo, Japan*

Received 18 July 2006; received in revised form 10 January 2007; accepted 24 January 2007

Abstract

Autism (MIM 209850) is a severe neurodevelopmental disorder characterized by disturbances in social interaction and communication, by repetitive body movements and restricted interests, and by atypical language development. Several twin and family studies have shown strong evidence for genetic factors in the etiology of autism. Glutamate is a major excitatory neurotransmitter in the human brain. Glutamate systems are involved in the pathophysiology of autism. There are many similarities between the symptoms evoked by glutamate antagonist treatment and symptoms of autism found in several human and animal studies. To elucidate the genetic background of autism, we analyzed the relationship between three single nucleotide polymorphisms (SNPs) of the Tachykinin 1 gene (TAC1) and autism, because TAC1 is located in the candidate region for autism and produces substance P and neurokinins. These products modulate glutamatergic excitatory synaptic transmission and are also involved in inflammation. Many different inflammation-related mechanisms could be involved in the autistic brain. Therefore, TAC1 may have some functions associated with the presumable pathophysiology of autism. We compared the allele and haplotype frequencies between autistic patients ($n = 170$) and normal controls ($n = 214$) in the Japanese population, but no significant difference was observed. Thus, the TAC1 locus is not likely to play a major role in the development of autism.

Keywords: Autistic disorder; Chromosome 7; TAC1; Genetic association; Glutamate system; Haplotype block

1. Introduction

Autism is a neurodevelopmental disorder characterized by early onset of the three cardinal symptoms: disturbance of social interaction, atypical language

* Corresponding author. Tel.: +81 3 5800 9263; fax: +81 42 379 4544.
E-mail address: PXX03135@nifty.ne.jp (T. Marui).

0387-7604/$ - see front matter © 2007 Elsevier B.V. All rights reserved.
doi:10.1016/j.braindev.2007.01.010

development, and restricted, repetitive, stereotyped patterns of behavior and interests [1]. The genetic involvement of autism has been supported by its higher concordance rates for monozygotic twins than for dizygotic [2,3] and the several chromosomal loci possibly linked to autism, including 7q22-q31 [1].

Glutamate is one of the neurochemicals speculated to contribute to the pathogenesis of autism, because (1) there are many similarities between the symptoms evoked by glutamate antagonist treatment and the symptoms of autism found in several human and animal studies [4]; (2) several neuropathological and brain-imaging studies of autistic patients have shown involvement of the cerebral regions where glutamatergic neurons originate [4]; (3) the mRNA levels of the α-amino-3-hydroxy-5-methyl-4-isoxazole propionic acid (AMPA) receptor increases in autistic subjects [5]; (4) the aspartate/glutamate carrier SLC25A12 gene and metabotropic glutamate receptor 8 gene have been reported to be associated with autism [6,7].

In this study, we focused on the Tachykinin 1 gene (TAC1; MIM162320) because it is located in 7q21-q22 and encodes a precursor containing substance P and other neurokinins (Neurokinin A, Neurokinin K, and Neuropeptide γ) [8], some of which are implicated in the modulation of glutamate-driven neurotransmission and excitotoxicity in the basal forebrain and other CNS regions [9]. Moreover, TAC1 mutant mice are less sensitive to nociceptive stimulation, which reminds us of some autistic patients ignorant of pain [4,11]. An increase in proinflammatory cytokines and the activation of microglia and astrocytes in the brain of autistic patients may be also associated with the inflammatory responses of TAC1 products [12].

Based on TAC1 biological information and its chromosomal location, we considered the gene worth analyzing as one of the autism candidate genes. In the present study, we tested for the presence of an association of three single nucleotide polymorphisms (SNPs) of TAC1, and haplotypes consisting of the SNPs, with autism, using case-control design.

2. Subjects and methods

The patients comprised 170 unrelated Japanese with autism (147 males and 23 females, mean age = 20.8 years within a range of 3–41 years). The patients were recruited from the outpatient clinics of the departments of psychiatry, Tokyo University Hospital and Tokai University Hospital, and seven daycare facilities for subjects with developmental disorders. All the hospitals and facilities were located around Tokyo. All the subjects met the DSM-IV criteria for autistic disorder. The diagnoses were made by one or two experienced child psychiatrists through interviews and reviews of clinical records. Apparent physical anomalies were not observed in the subjects. The controls consisted of 214 unrelated Japanese healthy volunteers (145 males and 69 females, mean age = 34.6 years within a range of 21–65 years). They were mainly recruited from the hospital and facility staff, and all of them resided in the same area (Kanto District or around Tokyo) as the patients. All the patients and controls were ethnically Japanese, with no parents or grandparents of ethnicity other than Japanese.

Confirmation of the diagnosis was conducted as follows. Semi-structured behavior-observation of the patients and interviews with them and their parents were conducted for most of the cases by two experienced child psychiatrists independently. At the interview with the parent(s), the Child Behavior Questionnaire Revised (CBQ-R) [10] was used to assist evaluation of autism-specific behavior and symptoms. After the initial observation and interview, we followed up by examining the patients' behavior and symptoms for several months (for at least 6 months in most of the cases) and those who were not considered to meet the DSM-IV criteria during the follow-up were excluded from the sample.

The present study was approved by the Ethical Committee, the Faculty of Medicine of the University of Tokyo and Tokai University. The objective of the present study was clearly expressed and written informed consent was obtained from all subjects and healthy volunteers.

Peripheral blood was obtained and genomic DNA was extracted using the standard phenol–chloroform

Table 1
Allele frequencies of 3 SNPs of the TAC1 gene in autism patients and controls

Locus	db SNP ID	Allele A/B[a]	Minor allele frequencies				χ^2	*P*-value	Odds ratio	95% confidence intervals		Location
			Patients		Controls					Lower	Upper	
			N	%	*N*	%						
SNP 1	rs2072100	C/T	107	31.8	136	32.2	0.01	0.91	1.02	0.75	1.38	int01
SNP 2	rs1229434	C/T	149	44.3	199	47.2	0.60	0.44	1.12	0.84	1.49	int06
SNP 3	rs1397202	A/G	68	20.1	82	19.2	0.09	0.76	0.95	0.66	1.35	int06

[a] Alleles "B" are minor alleles.

method. Single nucleotide polymorphisms (SNPs) were analyzed using the ABI 7900HT sequence detection system (Applied Biosystems, Foster City, CA, USA). Three SNPs of the TAC1 gene were selected from the list of Assays-on-Demand™ Products for the ABI 7900HT to cover the full length of the gene, considering minor allele frequencies indicated in the products list. The db SNP IDs of the SNPs are shown in Table 1.

Statistical analyses were performed using the SAS/Genetics 9.1 software (SAS Institute Inc., Cary, North Carolina, USA). The frequencies of alleles and genotypes of each SNP were compared between patients and controls using the χ^2 test. To further analyze the haplotype structure in our sample, we computed the pair-wise D' values that indicated the linkage disequilibrium (LD) between the SNPs. The frequencies of haplotypes consisting of SNPs, which were at a high linkage disequilibrium (haplotype block), were estimated. The exact P-values based on the likelihood ratio test with 10,000 permutations were calculated for comparison of the haplotype frequencies between patients and controls.

3. Results

The allele frequencies of the SNPs of the TAC1 gene are summarized in Table 1. No significant difference was observed in genotypic distributions (not shown in the tables) or allele frequencies of the three markers of the TAC1 gene between patients and controls. The minor allele frequencies of the SNPs were higher than 19% in all three SNPs. For all assayed SNPs, none of the SNPs deviated from Hardy–Weinberg equilibrium.

The pair-wise D' and r^2 values of the SNPs within the TAC1 gene are summarized in Table 2. Considering r^2, these three SNPs within the TAC1 gene were not in complete linkage disequilibrium with each other. However, all the pair-wise D' values of each SNP indicated 1.00, forming a haplotype block. Regarding the pair-wise D' values, therefore, three marker haplotypes of SNP1-3 (rs2072100, rs1229434, rs1397202), were tested.

The estimated haplotype frequencies are shown in Table 3. No significant difference was observed in the estimated haplotype distributions between patients and controls.

Table 2
The strength of LD (denoted as D′ and r2) between pairs of SNPs of TAC1 in autism patients (the lower diagonal) and controls (the upper diagonal)

SNP	1	2	3
D'			
1		1.00	1.00
2	1.00		1.00
3	1.00	1.00	
r_2			
1		0.53	0.11
2	0.60		0.22
3	0.12	0.20	

Table 3
Estimated frequencies and permutation P-values for association of major TAC1 haplotypes with rs2072100-rs1229434-rs1397202

Haplotype	Frequencies		χ^2	P-value
	Case	Control		
C-C-A	0.36	0.33	0.42	0.53
T-T-A	0.32	0.32	0.00	0.95
C-C-G	0.20	0.19	0.09	0.78
C-T-A	0.12	0.15	1.33	0.25

Global $P = 0.6958$

Haplotype frequencies were estimated >1%.

4. Discussion

We genotyped three SNPs within the TAC1 gene. No association was found in the allele and haplotype distributions between autistic patients and normal controls.

The 95% confidence intervals of the odds ratios were within 0.66 and 1.49 in all three SNPs of the gene. Considering the sample size and minor allele frequencies in the present study, our results might have adequate statistical power (>0.8) to contradict the effects of the gene with odds ratios of approximately 1.7 or more.

The TAC1 gene is located on 7q21.3 within the candidate region for autism and has 7 exons spanning approximately 8.4 kb of genomic DNA [11]. Neurokinin A, neuropeptide K, and neuropeptide γ, as well as Substance P, are produced from the TAC1 gene as a result of differential splicing and posttranslational processing [12] (Fig. 1). Substance P and other neurokinins are known as a mediators of pain and inflammation. They are produced in nociceptive primary sensory neurons and in many brain regions involved in pain signaling. Pain behavior evoked by thermal, mechanical, and chemical stimulation of somatic and visceral tissues were all reduced in the TAC1 mutant mice [6].

Besides pain and inflammation, the concentration of Substance P was elevated in the cerebrospinal fluid of depressed patients, and in the brain of a rat model of depression. Limbic structures contain a high density of Substance P terminals and Neurokinin 1 receptor sites. The tachykinin system therefore may play an important role in the regulation of emotional states and the development of anxiety disorders and depression [8].

In the Rett syndrome included in pervasive developmental disorders (PDD) with autistic symptoms, reduced expression of the TAC1 gene products was reported [13,14]. This fact may suggest that the TAC1 gene might not be implicated in the whole spectrum of PDD.

Nontheless, several facts, including decreased pain sensitivity, brain inflammation, and association of the

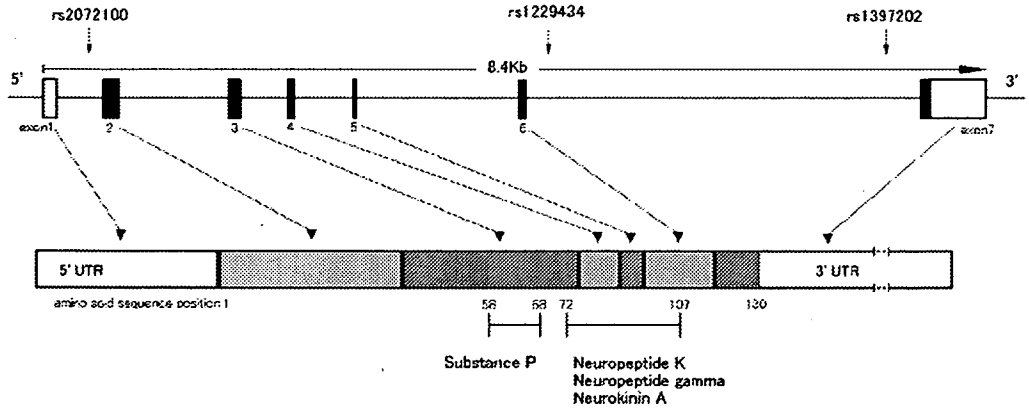

Fig. 1. This figure shows the TAC1 gene structure and positions of the SNPs (presented from 5′ to 3′ of the gene). All SNPs are denoted numerically with reference to Table 1. The vertical black bars indicate exons. Open boxes indicate the 5′ and 3′ untranslated regions. A horizontal line between the exons depicts introns. The TAC1 gene product is also indicated. Neurokinins are produced as a result of differential splicing and posttranslational processing of the product.

TAC1 gene with the glutamate system, suggested that Substance P or other neurokinins, which are products of the TAC1 gene, might contribute to the etiology of a part of autism. Although our data denied the association of the TAC1 gene with autism, these facts possibly support the necessity for this study.

The controls in this study were not age-matched to the patients. However, this is not likely to affect the result, considering the strong effect of genetic factors in autism compared with the rather small effect of environmental factors [2,15].

Another concern may be the population stratification of the sample, which could affect the results of studies in case-control design. This may not, however, significantly affect the present result, because the Japanese population is highly homogeneous, due to no major immigration for more than a thousand years, compared with the European or North American population. No subjects in this study had parents or grandparents of ethnicity other than Japanese.

In conclusion, we analyzed three SNPs in the TAC1 gene to determine whether there exists an association of TAC1 with autism using case-control design. To our knowledge, this is the first study that has examined the role of TAC1 polymorphisms in autism. No association was observed in this study.

References

[1] Folstein SE, Rosen-Sheidley B. Genetics of autism: complex aetiology for a heterogeneous disorder. Nat Rev Genet 2001;2:943–55.

[2] Bailey A, Le Couteur A, Gottesman I, Bolton P, Simonoff E, Yuzda E, et al. Autism as a strongly genetic disorder: evidence from a British twin study. Psychol Med 1995;25:63–77.

[3] Steffenburg S, Gillberg C, Hellgren L, Andersson L, Gillberg IC, Jakobsson G, et al. A twin study of autism in Denmark, Finland, Iceland, Norway and Sweden. J Child Psychol Psychiatry 1989;30:405–16.

[4] Ramoz N, Reichert JG, Smith CJ, Silverman JM, Bespalova IN, Davis KL, et al. Linkage and association of the mitochondrial aspartate/glutamate carrier SLC25A12 gene with autism. Am J Psychiatry 2004;161:662–9.

[5] Serajee FJ, Zhong H, Nabi R, Huq AH. The metabotropic glutamate receptor 8 gene at 7q31: partial duplication and possible association with autism. J Med Genet 2003;40:e42.

[6] Cao YQ, Mantyh PW, Carlson EJ, Gillespie AM, Epstein CJ, Basbaum AI. Primary afferent tachykinins are required to experience moderate to intense pain. Nature 1998;392:390–4.

[7] Zhang JP, Wei LC, Cao R, Chen LW. Differential co-expression of AMPA receptor subunits in substance P receptor-containing neurons of basal forebrain regions of C57/BL mice. Neurochem Int 2006;49:319–26.

[8] Bilkei-Gorzo A, Racz I, Michel K, Zimmer A. Diminished anxiety- and depression-related behaviors in mice with selective deletion of the Tac1 gene. J Neurosci 2002;22:10046–52.

[9] Vargas DL, Nascimbene C, Krishnan C, Zimmerman AW, Pardo CA. Neuroglial activation and neuroinflammation in the brain of patients with autism. Ann Neurol 2005;57:67–81.

[10] Izutsu T, Osada H, Tachimori H, Naganuma Y, Kato S, Kurita H. The usefulness of the child behavior questionnaire revised (CBQ-R) as a supplementary scale for diagnosis of pervasive developmental disorders. Rinsyo-Seishin Igaku 2001;30:525–32, in Japanese.

[11] Ogden CA, Rich ME, Schork NJ, Paulus MP, Geyer MA, Lohr JB, et al. Candidate genes, pathways and mechanisms for bipolar (manic-depressive) and related disorders: an expanded convergent functional genomics approach. Mol Psychiatry 2004;9:1007–29.

[12] Krause JE, Chirgwin JM, Carter MS, Xu ZS, Hershey AD. Three rat preprotachykinin mRNAs encode the neuropeptides substance P and neurokinin A. Proc Natl Acad Sci USA 1987;84:881–5.

[13] Deguchi K, Antalffy BA, Twohill LJ, Chakraborty S, Glaze DG, Armstrong DD, et al. immunoreactivity in Rett syndrome. Pediatr Neurol 2000;22:259–66.

[14] Matsuishi T, Nagamitsu S, Yamashita Y, Murakami Y, Kimura A, Sakai T, et al. Decreased cerebrospinal fluid levels of substance P in patients with Rett syndrome. Ann Neurol 1997;42:978–81.

[15] Szatmari P, Jones MB, Zwaigenbaum L, MacLean JE. Genetics of autism: overview and new directions. J Autism Dev Disord 1998;28:351–68.

Available online at www.sciencedirect.com
ScienceDirect
Neuroscience Research 57 (2007) 504–512
Neuroscience Research
www.elsevier.com/locate/neures

Multiple-time replicability of near-infrared spectroscopy recording during prefrontal activation task in healthy men

Toshiaki Kono *, Koji Matsuo, Koichi Tsunashima, Kiyoto Kasai **, Ryu Takizawa, Mark A. Rogers, Hidenori Yamasue, Tetsu Yano, Yuji Taketani, Nobumasa Kato

Department of Neuropsychiatry, Graduate School of Medicine, The University of Tokyo, 7-3-1 Hongo, Bunkyo-ku, Tokyo 113-8655, Japan

Received 8 March 2006; accepted 12 December 2006
Available online 22 December 2006

Abstract

Near-infrared spectroscopy (NIRS) has the potential for clinical application in neuropsychiatry because it enables non-invasive and convenient measurement of hemodynamic response to cognitive activation. Using 24-channel NIRS in 12 healthy men, we examined the replicability of oxy- and deoxy-hemoglobin concentration ([oxyHb], [deoxyHb]) changes in the prefrontal cortex during the category fluency task over four repeated sessions (each 1-week apart). Multiple methods were employed to evaluate the replicability of magnitude, location, and time course of the NIRS signals ([oxyHb], [deoxyHb]). Task performances did not differ significantly across sessions, nor were they significantly correlated with NIRS signals. Repeated measures ANOVA and variance component analysis indicated high replicability of magnitude for both NIRS measures, whereas the effect sizes of between-session differences in [oxyHb] were not negligible. The number and spatial location of significantly activated channels were sufficiently replicable for both measures, except that the across-session overlap of significantly activated channels was weak in [deoxyHb]. The time course of the activation was acceptably replicable in both measures. Taken together, these findings suggest there is considerable replicability of multiple-time measurements of prefrontal hemodynamics during cognitive activation in men. Further studies using different conditions or assessing sensitivity to longitudinal changes following interventions are necessary.

Keywords: Category fluency; Hemoglobin concentration; Practice effect; Prefrontal; Repeatability; Repeated measurement; Reproducibility; Test–retest

1. Introduction

Near-infrared spectroscopy (NIRS) is an optical technique which can non-invasively measure changes in the hemoglobin oxygenation state in human brain (Jobsis, 1977). NIRS was originally developed for clinical monitoring of tissue oxygenation (Wyatt et al., 1986); however, it has been increasingly utilized as a neuroimaging technology. NIRS takes advantage of the principle that near-infrared light is absorbed by oxygenated (oxyHb) and deoxygenated hemoglobin (deoxyHb) but not so much by other tissues. An NIRS measurement apparatus needs a pair of optodes, one emitter and one detector, placed a few centimeters apart from each other. Near-infrared light exiting the emitter optode positioned on the scalp travels through skin, skull, and brain, and is multiply scattered and partially absorbed. The residual light not absorbed by tissue exits the head and can then be detected by the detector optode (Obrig et al., 2000). Therefore, the brain region measured is supposed to be a 'banana-shaped' area between the two optodes (Gratton et al., 1994) with a depth of 0.9 cm beneath the brain surface (Villringer et al., 1997). NIRS uses two different wavelengths of near-infrared light, and can calculate changes in the concentration of oxyHb ([oxyHb]) and deoxyHb ([deoxyHb]) by means of the modified Beer–Lambert law which describes the relationship between the intensities of incident and detected light, and the fact that the absorption characteristic determined as a function of wavelength differs between oxyHb and deoxyHb.

Although the spatial resolution of NIRS is inferior to those of other functional neuroimaging methodologies such as positron-emission tomography (PET) and functional magnetic resonance imaging (fMRI), NIRS has a high time resolution of less than 0.01 s, and subjects can be scanned under natural

* Corresponding author. Tel.: +81 3 5800 9263; fax: +81 3 5800 6894.
** Co-corresponding author. Tel.: +81 3 5800 9263; fax: +81 3 5800 6894.
E-mail addresses: tkono-tky@umin.ac.jp (T. Kono), kasaik-tky@umin.ac.jp (K. Kasai).

0168-0102/$ – see front matter
doi:10.1016/j.neures.2006.12.007

conditions (Miyai et al., 2001). Thus, NIRS is suitable for measuring change in cerebral blood volume (CBV) during cognitive tasks. With these advantages, several studies using NIRS have demonstrated an increase in [oxyHb] in the prefrontal cortex in response to cognitive activation in healthy subjects (Hoshi and Tamura, 1993; Villringer et al., 1993, 1997; Hock et al., 1995; Fallgatter and Strik, 1997, 1998; Hoshi et al., 2000) as well as differences in patterns of activation between healthy subjects and those with neuropsychiatric disorders (Okada et al., 1994, 1996; Hock et al., 1997; Fallgatter and Strik, 2000; Matsuo et al., 2000, 2002, 2004; Watanabe et al., 2003; Herrmann et al., 2004).

NIRS also has an advantage that repeated measurements in an individual are possible because it is non-invasive and NIRS devices are relatively small and portable. Hence, NIRS has the potential to be applied in clinical testing in which cognitive activations induced by the same kind of task are monitored at short-term multiple time-points (e.g., before and after a certain therapeutic intervention). However, the possibility for practice effects upon repeated testing with the same cognitive task must be considered. Previous PET and fMRI studies have demonstrated practice effects as a decrease (Jansma et al., 2001), an increase (Karni et al., 1995; Honda et al., 1998), or combination of both (Hempel et al., 2004) in cortical activation. The location of activation has also been observed to change in response to repeated testing with cognitive activation tasks (Raichle et al., 1994; Poldrack et al., 1998; Poldrack and Gabrieli, 2001).

The replicability of NIRS measures (i.e. oxyHb, deoxyHb, and totalHb (sum of oxyHb and deoxyHb)), was examined by Plichta et al. (2006). Event-related cerebral hemodynamics in the occipital cortex activated by a visual stimulation was assessed twice at an interval of 3 weeks in 12 subjects. They found good replicability at the group level in terms of single measure intraclass correlation coefficients (ICC) (0.72 and 0.52 for oxyHb and deoxyHb, respectively) when averaged across the significantly activated channels in the first session, whereas the results at the level of individual subjects were less consistent (mean Pearson correlation coefficients for oxyHb of 0.63 with 3 out of 12 subjects resulting in values around 0.4). Van de Ven et al. (2001) examined the replicability of CBV as measured by NIRS applying controlled desaturation (the O_2-method), and yielded a mean coefficient of variation (CV) of 10.0–12.6%. Another NIRS study by Claassen et al. (2006) also reported good replicability of CBV in 16 healthy elderly subjects using the O_2-method. They found CVs of 12.5% for 'repeatability' (between tests interval: 2 min), 11.7% for 'short-term reproducibility' (intervals of 20 and 40 min), and 15% for 'long-term reproducibility' (interval > 2 weeks).

To our knowledge, only one study (Watanabe et al., 2003) has preliminarily reported replicability of [oxyHb] change in the prefrontal cortex during cognitive activation tasks with a mean interval of 205 days in five healthy adults, and reported an acceptable replicability (ICC: 0.42 and 0.87 for design and letter fluency test, respectively). To date, however, no data exist concerning replicability of hemodynamic response induced by a cognitive activation task assessed systematically using NIRS. Accordingly, in the present study, we examined the replicability of hemoglobin concentration ([Hb]) change in the prefrontal cortex during a cognitive activation task over four repeated sessions (each 1-week apart) in healthy men using NIRS.

2. Materials and methods

2.1. Subjects

Twelve healthy male volunteers (age, mean [S.D.] = 28.1 [2.6] years) participated in the experiment. All were strongly right-handed as assessed with the Edinburgh Inventory (Oldfield, 1971) (laterality index > +85). They were examined by a trained psychiatrist (K.M.) using the Mini International Neuropsychiatric Interview (Sheehan et al., 1998) and were confirmed not to have any histories of neuropsychiatric disorders. All experiments in this study were conducted in accordance with the Declaration of Helsinki. Every subject was given a complete explanation of the study sufficient to their understanding, after which their written informed consent was obtained. This study was approved by the Ethical Committee of the Faculty of Medicine, The University of Tokyo (No. 670).

2.2. NIRS apparatus and measurement conditions

NIRS measurements were performed using a 24-channel instrument (ETG-100, Hitachi Medical Corporation, Tokyo, Japan). Two plastic shells each with nine individual optodes were carefully fixed with elastic straps on the left and the right forehead symmetrically. The most anterior row of optodes was

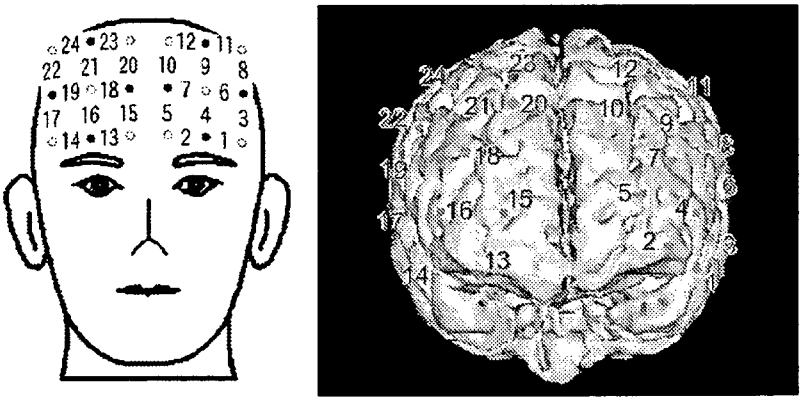

Fig. 1. Typical positions of the 24 points as indicated with digits measured by NIRS. Open and solid circles represent emitter and detector optodes, respectively (left). The positions are superimposed with red spots on a magnetic resonance image of a reconstructed cerebral cortex (right).

positioned along the Fp_1–Fp_2 line, according to the international 10/20 system used in electroencephalography. Typical positions of the 24 measurement points are indicated by superimposing them onto the cortical surface of a 3D-MRI image (Fig. 1). The subjects sat on a comfortable chair with their eyes open throughout the measurements.

2.3. Cognitive activation task

The category fluency task (CFT) was adopted as a cognitive activation task, and the speech–sound repetition task (SRT) was applied as a control task for the purpose of controlling for the effect of speaking. The CFT is a version of the verbal fluency task, a popular task for activating the prefrontal cortex (Audenaert et al., 2000). The subjects heard an audiotaped instruction, and were asked to repeat syllables /a/, /i/, /u/, /e/, and /o/ at approximately the same speed as an audiotaped sample in the SRT, and to generate as many words belonging to the designated category (e.g., fruits, kitchenware) as possible in the CFT. Task performance was defined as the number of correctly generated words during the CFT.

2.4. Experimental procedure

We performed four sessions of NIRS measurement at intervals of 1 week (mean [S.D.] = 7.1 [0.8] days) for each subject. A session of NIRS measurement proceeded consecutively in the following order: (1) instruction, (2) rest (2 min), (3) the SRT (1 min), (4) the CFT (1 min), and (5) the SRT (1 min). In the CFT, we designated two categories in each session. The two categories changed in turn every 30 s during the 1-min task, to reduce the time when the subjects were silent. We prepared four combinations of categories (fruits (30 s)/kitchenware (30 s); vegetables/clothes; birds/vehicles; and fishes/sports) and used each of them once

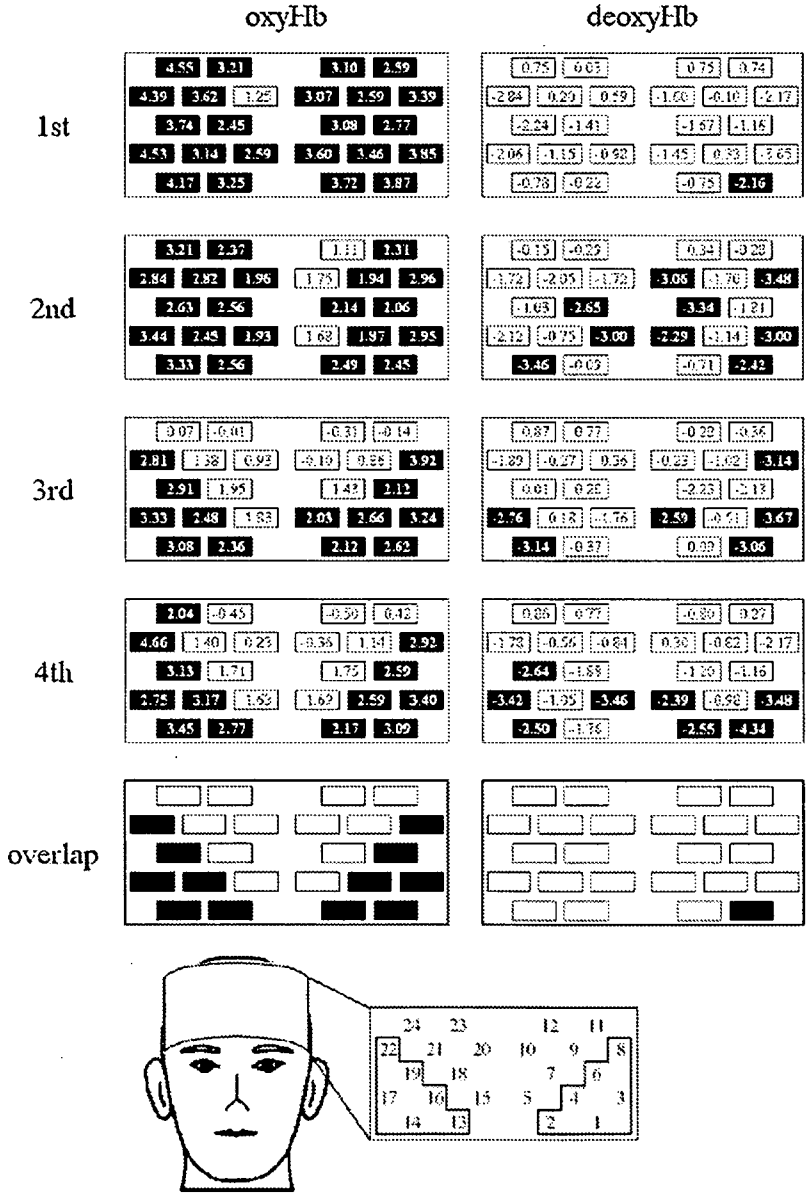

Fig. 2. Location of channels significantly activated and t-values for each NIRS measure for each recording session and those activated consistently in every session (overlap). Channels indicated as solid rectangles with t-values written in white letters in them were significantly activated, whereas those indicated as open rectangles with t-values in black letters were not. The channels are located similarly as shown in a rectangle below with the numbers of channels (the surrounded numbers correspond the channels within the region of interest).

with each subject, i.e. every subject experienced all eight categories in the four sessions. The order of the combinations used was randomized across the subjects.

2.5. NIRS data analyses

The NIRS data were modified to exclude short-term motion artifacts using moving average method with a window of 1 s. The obtained data were analyzed with the 'integral mode': the pre-task baseline was defined as the mean across 5 s just before the activation period (time 55–60 s of the former SRT), the post-task baseline as the mean across 5 s beginning 50 s after the activation period ended (time 50–55 s of the latter SRT), and linear fitting was performed on the data between the two baselines. Therefore, the CFT-related activation is corrected for the effect of speaking in all the NIRS data used in the analyses. Previous studies examining the relationship between NIRS signals and blood oxygenation level-dependent (BOLD) signal, measured by fMRI, during cognitive tasks have produced inconsistent results. Strangman et al. (2002) found the best correlation with oxyHb, while Huppert et al. (2006) found the best correlation with deoxyHb. Thus, we analyzed both oxyHb and deoxyHb measures throughout the analyses.

2.6. Statistical analysis

The analyses were performed with a statistical software package 'SPSS for Windows 10.1J' (SPSS Japan, Tokyo, Japan). The alpha level was set at 0.05 in the tests for statistical significance and, except for finding significantly activated channels, was not corrected for multiple comparisons because of an interest to confirm equivalence. We adopted the false discovery rate method (Singh and Dan, 2006) for multiple comparison setting q at 0.05 in finding significantly activated channels.

2.6.1. Task performance

Task performances were compared across types of category or sessions using one-way repeated measures analysis of variance (ANOVA). Then, an effect size (ES) was calculated for a difference in task performance between every two separate sessions. For ES, we regarded values of $\geq$0.65 as large, $\geq$0.35 but <0.65 as moderate, and <0.35 as small, in consideration of standard convention (Cohen, 1977).

2.6.2. Significance of NIRS signal change relative to baseline

We performed one sample t-tests (one-tailed) for [oxyHb] and [deoxyHb] changes averaged across the CFT activation period in every channel, and defined the channels in which the averaged [Hb] change was significantly positive and negative as significantly activated ones for oxyHb and deoxyHb, respectively. Then, as described in the results section, we defined a region of interest (ROI) as the channels consistently significantly activated for oxyHb in every session. The resulting ROI (left hemisphere: channels #1, 2, 3, 4, 6, 8; right hemisphere: #13, 14, 16, 17, 19, 22) (Fig. 2) was further used for analyzing the replicability of NIRS measures.

2.6.3. Correlation between task performance and NIRS signals

Pearson's correlation coefficients were calculated between task performance and averaged [oxyHb] and [deoxyHb] changes across the ROI in each single session and the four sessions combined.

2.6.4. Replicability in magnitude of activation

We evaluated the replicability of the magnitude of NIRS signal changes in three different ways.

First, we tested the differences in the averaged [oxyHb] and [deoxyHb] changes during the CFT over the four sessions using repeated measures ANOVA, for each single channel within the ROI independently and for the mean values of the six channels in each hemisphere (two within-subject factors of session and hemisphere). The absolute values of magnitudes of [Hb] change were used as both positive (for increased [Hb]) and negative (for decreased [Hb]) values.

Second, we estimated how much of the total variance of each NIRS measure could be attributed to each component of between-subject, between-session, and within-subject variance, using the data averaged for the ROI (variance component analysis).

Third, we calculated effect sizes (ESs) of all the relevant mean differences.

2.6.5. Spatial replicability

We then evaluated spatial replicability of significantly activated channels in two ways.

First, we calculated replicability indices (R_{quantity} and R_{overlap}) for each NIRS measure to quantify the replicability, extending Rombouts' ones originally defined for data in two sessions (Rombouts et al., 1997):

$$R_{\text{quantity}} = 1 - \frac{\sum_{i \neq j} |X_i - X_j|}{\sum_{i \neq j} (X_i + X_j)}$$

and

$$R_{\text{overlap}} = \frac{4X_{\text{overlap}}}{\sum_i X_i}$$

where X_i (X_j) represents the number of the activated channels in the ith (jth) session, and X_{overlap} represents that in every session consistently. Both indices can vary between 0 and 1, and high R_{quantity} and R_{overlap} indicate high replicability in terms of quantity and location, respectively, of significantly activated channels. For R_{quantity} and R_{overlap}, values of $\geq$0.8 are considered as highly replicable, $\geq$0.6 but <0.8 as moderately replicable, and <0.6 as weakly replicable. We also calculated R_{quantity} and R_{overlap} for all 24 measured channels for reference, in addition to those for the ROI.

Second, we estimated 'activation centers' in each hemisphere for each NIRS measure using the averaged [Hb] changes during the CFT in the six channels within the ROI. First of all, we assigned a frame of reference to each hemisphere such that the abscissa and the ordinate coincide with the middle horizontal and vertical rows of optodes, respectively (the origin coincides with the midmost emitter optode), assuming that the measurement areas exist on the planes composed by the axes and that the distances of any horizontally (or vertically) neighboring optodes are constant (=1). Consequently, the distance between nearest (obliquely neighboring) channels equals 1/(square root of 2) ($\approx$0.71). An activation center was defined as the mean of the coordinates of each channel weighted with the magnitude of the averaged [Hb] change in the channel. The coordinates of the activation center (x_c, y_c) were calculated as follows:

$$x_c = \frac{\sum_i x_i m_i}{\sum_i m_i}$$

$$y_c = \frac{\sum_i y_i m_i}{\sum_i m_i}$$

where m_i and (x_i, y_i) represent the magnitude of the averaged [Hb] change in and the coordinates of the ith channel, respectively. We calculated all the relevant distances of activation centers in each hemisphere for each NIRS measure.

2.6.6. Replicability in time course

We investigated temporal replicability by calculating Pearson's correlation coefficients between time series of the averaged [Hb] changes across the ROI in all the combinations of sessions for each NIRS measure.

3. Results

3.1. Task performance

Task performance of the CFT was not significantly different across types of category (mean [S.D.]; fruits and kitchenware, 20.3 [5.0]; vegetables and clothes, 22.1 [4.2]; birds and vehicles, 20.3 [5.1]; fishes and sports, 22.9 [5.8]; $F[3,33] = 2.570$, $p = 0.071$) or across sessions (1st, 21.4 [4.9]; 2nd, 21.5 [4.8]; 3rd, 22.0 [5.6]; 4th, 20.7 [5.3]; $F[3,33] = 0.374$, $p = 0.772$). The ESs were small for all the relevant mean differences (Table 1).

3.2. Significance of NIRS signal change relative to baseline

The t-tests show that, for [oxyHb], there were many channels showing significant activation associated with the cognitive

Table 1
Effect sizes of all the relevant mean differences in task performance and in averaged hemoglobin concentration change (mean across 12 channels within the region of interest) during the category fluency task

	1st–2nd	1st–3rd	1st–4th	2nd–3rd	2nd–4th	3rd–4th
Task performance	0.02	0.23	0.15	0.11	0.21	0.30
oxyHb	0.14	0.72	0.60	0.47	0.40	0.14
deoxyHb	0.11	0.03	0.08	0.12	0.00	0.18

task relative to baseline, while channels showing significant decreases were relatively sparse for [deoxyHb] (Fig. 2). The left hemisphere channels #1, 2, 3, 4, 6, 8, and the corresponding mirror symmetrical right hemisphere channels #13, 14, 16, 17, 19, 22 were consistently significantly activated for oxyHb in every session. Consequently, we defined these 12 channels as the ROI.

3.3. Correlation between task performance and NIRS signal

Pearson's correlation coefficients between task performance and averaged [Hb] changes were not significant for [oxyHb] ($p > 0.29$) or [deoxyHb] ($p > 0.15$).

3.4. Replicability in magnitude of activation

In the repeated measures ANOVA, the averaged [Hb] change during the CFT was not significantly different across the four

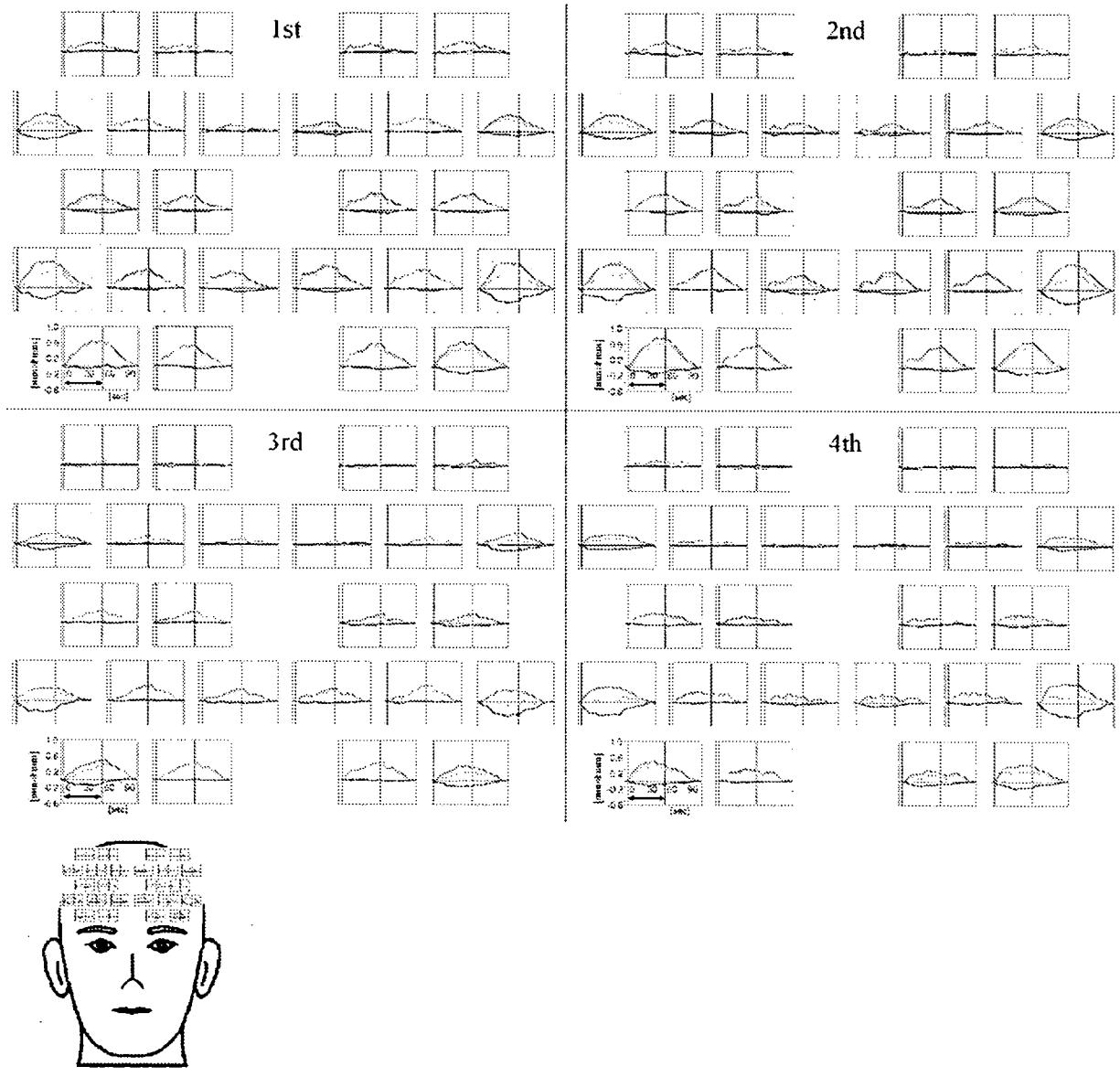

Fig. 3. Grand average waveforms of hemoglobin concentration ([Hb]) changes during the category fluency task (CFT) across all the subjects drawn for every channel in each session. [oxyHb], [deoxyHb], and [totalHb] were colored in red, blue, and green, respectively. Graphs for each channel are located similarly as shown below. The arrow drawn between the two vertical lines indicates the CFT activation period. [Hb] changes are corrected for the effect of simple speaking, using linear fitting between the pre-task baseline (the initial 5 s of the time course shown in the graphs) and the post-task baseline (the last 5 s).

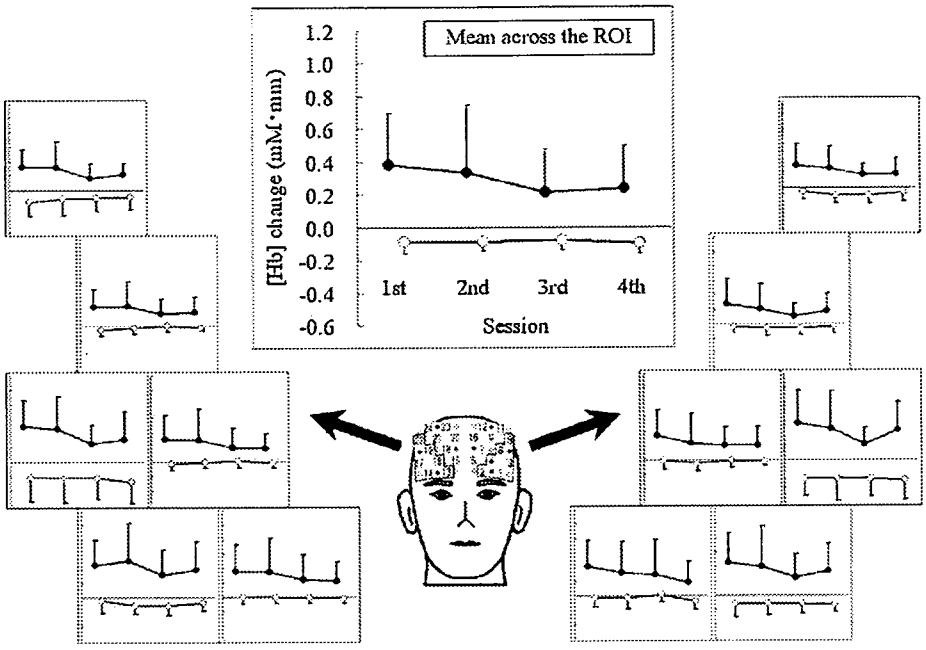

Fig. 4. Alternation in the averaged hemoglobin concentration changes during the category fluency task over the four sessions in each channel and in the mean across the region of interest. Solid and open circles represent oxygenated and deoxygenated hemoglobin, respectively. The error bars represent standard deviations.

Table 2
Number of significantly activated channels and replicability indices

NIRS measure	1st	2nd	3rd	4th	Overlap[a]	$R_{quantity}$[b]	$R_{overlap}$[b]
For the ROI							
oxyHb	12	12	12	12	12	1.00	1.00
deoxyHb	1	4	5	6	1	0.67	0.25
For all 24 channels							
oxyHb	23	20	13	13	12	0.82	0.70
deoxyHb	1	9	6	8	1	0.64	0.17

[a] The value is the number of channels activated significantly over the four sessions consistently.

[b] $R_{quantity}$ and $R_{overlap}$ are replicability indices of the quantity and the location of significantly activated channels, respectively. The formulae to calculate them are described in Section 2.6.5.

sessions in any channel within the ROI in either of oxyHb or deoxyHb (Figs. 3 and 4). In the two-way repeated measures ANOVA in consideration of laterality, there was no significant main effect of session ($F[3,33] = 2.270, 0.115$; $p = 0.099, 0.951$, for oxyHb and deoxyHb, respectively) or hemisphere ($F[1,11] = 0.374, 0.237$; $p = 0.553, 0.636$), or interaction of session and hemisphere ($F[3,33] = 0.690, 0.149$; $p = 0.565, 0.929$).

The results of variance component analysis revealed that the between-subject component contributed 66.5% of the total variance of [oxyHb] change (the proportion of between-subject component to the total variance equals single measure ICC, which means ICC = 0.665 for oxyHb), whereas the between-session component contributed only 2.9%. The within-subject component contributed the remaining 30.6%. In deoxyHb, interestingly, between-session component did not contribute to the total variance at all (0.0%), and the contribution of the between-subject component (36.7%) was conversely smaller than that of the within-subject component (63.3%).

The ESs of all the relevant mean differences in [Hb] changes were moderate to large in some combinations of sessions for [oxyHb], whereas these were consistently small for [deoxyHb] (Table 1).

3.5. Spatial replicability

$R_{quantity}$ and $R_{overlap}$ for the ROI were overall moderate to high, except for the weak $R_{overlap}$ for [deoxyHb]. Those for all the measured channels were similarly moderate to high, except for the weak $R_{overlap}$ for [deoxyHb] (Table 2).

Table 3
Mean [S.D.] values in all the relevant distance between 'activation centers' in each hemisphere

NIRS measure	Hemisphere	1st–2nd	1st–3rd	1st–4th	2nd–3rd	2nd–4th	3rd–4th
oxyHb	Left	0.26 [0.26]	0.33 [0.27]	0.39 [0.40]	0.31 [0.25]	0.24 [0.31]	0.38 [0.37]
	Right	0.20 [0.14]	0.25 [0.16]	0.29 [0.26]	0.19 [0.16]	0.30 [0.36]	0.26 [0.30]
deoxyHb	Left	0.23 [0.18]	0.33 [0.24]	0.38 [0.43]	0.31 [0.19]	0.38 [0.28]	0.27 [0.23]
	Right	0.26 [0.22]	0.38 [0.21]	0.35 [0.22]	0.36 [0.21]	0.33 [0.23]	0.30 [0.15]

Distances are expressed in relative values defined so that the distance between neighboring optodes (approximately 3 cm) equals 1.

Table 4
Mean [S.D.] values of all the relevant Pearson's correlation coefficients between time courses of hemoglobin concentration change

NIRS measure	1st–2nd	1st–3rd	1st–4th	2nd–3rd	2nd–4th	3rd–4th
oxyHb	0.62 [0.33]	0.65 [0.28]	0.45 [0.45]	0.43 [0.50]	0.43 [0.39]	0.35 [0.46]
deoxyHb	0.47 [0.53]	0.53 [0.37]	0.57 [0.29]	0.41 [0.39]	0.45 [0.47]	0.51 [0.36]

The mean distances of 'activated centers' ranged between 0.2 and 0.4 in both hemispheres in every combination of sessions for oxyHb and deoxyHb, without remarkable variation (Table 3).

3.6. Replicability in time course

Pearson's correlation coefficients between the time courses of [Hb] changes in every two of the four sessions were acceptable for all combinations (on average across the subjects, $r > 0.35$, d.f. = 599, $p < 0.001$) (Table 4).

4. Discussion

We evaluated the replicability of magnitude, location, and time course of NIRS signals ([oxyHb], [deoxyHb]) in the prefrontal cortex during cognitive activations over four repeated sessions employing multiple methods. In summarizing our results, repeated measures ANOVA and variance component analysis indicated high replicability of magnitude for both NIRS measures, whereas the effect sizes of between-session differences in [oxyHb] were not negligible. The number and spatial location of significantly activated channels were sufficiently replicable for both measures, except for the across-session overlap of significantly activated channels being relatively weak in [deoxyHb]. The time course of the activation was acceptably replicable in both measures. Taken together, these findings suggest considerable replicability for multiple-time measurements of prefrontal [oxyHb] and [deoxyHb] changes during cognitive activation in men.

Before discussing the replicability of NIRS signals any further, we should assess the effect of task performance. However, task performance was not significantly different across sessions. Moreover, there was no significant correlation between task performance and NIRS signals. Therefore, we can conclude that there was no meaningful effect of task performance on the NIRS data.

The repeated measures ANOVA and variance component analysis showed that the magnitudes of [oxyHb] and [deoxyHb] changes during the CFT activation were quite replicable. However, moderate to large ESs for [oxyHb] in some combinations of sessions (1st to 3rd; 1st to 4th; 2nd to 3rd; 2nd to 4th) indicated that the conclusions for the replicability of magnitude of [oxyHb] change may not be definitive.

In previous fMRI studies using cognitive activation tasks, Langenecker and Nielson (2003) demonstrated comparable magnitude of activation across two separate sessions of the Go/No-go, with an exception of stronger activation at the first test than at the retest in some frontal parts which was explained by possible extraneuronal factors such as signal-to-noise ratio or task experience. Wei et al. (2004) observed a larger contribution to variation in activation during the two-back verbal working memory task from between-subject variation than from within-subject variation (including between-session variation), although they observed a session effect as well as a subject effect in the dorsolateral prefrontal cortex that might occur as a result of difficulty in defining the region. They concluded that the findings indicate a reasonable replicability of cognitive activation over sessions.

The present study replicated the above-mentioned study by Wei et al. (2004) in terms of a large contribution of between-subject effect to the total variance in cerebral activation. However, we cannot compare the current findings directly with the previous studies because the scanning conditions are heterogeneous in multiple aspects. On that point, the study by Watanabe et al. (2003) mentioned in Section 1 to the present paper is relevant to the present study in terms of the homogenous modality (NIRS) and activation task used (fluency task), whereas the inter-session intervals were variable. As compared with the high ICC in the LFT (0.871) demonstrated in their study, the value of ICC in the CFT in the present study (0.665) is inferior. However, it may be attributed to the shorter measurement intervals in the present study, because practice effects are liable to carry over with short intervals, making cognitive activation smaller.

Concerning spatial replicability of significantly activated channels, the quantity replicability (evaluated as $R_{quantity}$) was moderate to high in both NIRS measures, whereas the location replicability (evaluated as $R_{overlap}$) was lower in deoxyHb, for not only the ROI but also all the measured channels. The spatial reliability in terms of 'activation center' was well replicated over the sessions. Our results indicate that [oxyHb] can be considered as a more replicable NIRS measure in terms of significantly activated channels than [deoxyHb]. However, a caution should be mentioned in the interpretation of the replicability of [deoxyHb], because the significantly activated channels for [deoxyHb] themselves were sparse. Thus, the activation task in our study may not be best suited for evaluating the replicability of [deoxyHb] in repeated measurements. Since Rombouts et al. (1997) introduced $R_{quantity}$ and $R_{overlap}$, similar results have been replicated in a number of fMRI and NIRS studies employing visual stimulation (e.g., Rombouts et al., 1997; Miki et al., 2000; Plichta et al., 2006). Moreover, Harrington et al. (2006) also demonstrated a higher $R_{quantity}$ as compared with $R_{overlap}$ using cognitive tasks. With regard to 'activation centers', the current result replicated a previous NIRS study by Sato et al. (2006) which demonstrated a maximum mean distance between activation centers in two sessions of 18.6 mm (=0.62) in the sensorimotor cortex during visual stimulation. On the other hand, alternation in activated regions accompanied by repeated measurements has been reported in cognitive activation task